Supporting Information

Insights into the photoinduced anion translocation of the Donor-π-Acceptor^{+}(ion)$^{-}$ molecules

Hao-Ting Qu,[a] Iida Partanen,[b] Kai-Hsin Chang,[a] Yan-Ding Lin,[a] Igor O. Koshevoy,[b,*] Andrey Belyaev,[b,c,*] and Pi-Tai Chou,[a,*]

[a] Hao-Ting Qu, Dr. Kai-Hsin Chang, Prof. Pi-Tai Chou
Department of Chemistry, National Taiwan University, Taipei, Taiwan 10617, ROC
E-mail: chop@ntu.edu.tw
[b] Iida Partanen, Prof. I. O. Koshevoy, Dr. Andrey Belyaev
Department of Chemistry, University of Eastern Finland, Yliopistokatu 7, 80101 Joensuu, Finland
E-mail: igor.koshevoy@uef.fi ; andrei.beliaev@uef.fi
[c] Dr. Andrey Belyaev
Department of Chemistry/Nanoscience Center, University of Jyväskylä, Survontie 9C, 40014 Jyväskylä, Finland
E-mail: andrei.a.beliaev@jyu.fi

1.Synthetic details

General comments

7-Bromo-*N*,*N*-diphenyl-9,10-dihydrophenanthren-2-amine,[1] [4-(diphenylamino) phenyl]boronic acid[2], 4'-bromo-*N*,*N*-bis(4-(*tert*-butyl)phenyl)-[1,1'-biphenyl]-4-amine[3], 4-bromo-4′-(*N,N*-diphenylamino)-biphenyl[4], 4'-bromo-*N*,*N*-dimethyl[1,1'-biphenyl]-4-amine[5], [4-(9H-carbazol-9-yl) [1,1'-biphenyl]-4-yl]triphenyl-phosphoniumbromide and **2[OTf]** [6]were synthesized according to the published literature. Tetrahydrofuran (THF), toluene and diethyl ether were distilled over Na-benzophenone ketyl under a nitrogen atmosphere prior to use. Other reagents and solvents were used as received. The solution ^{1}H, ^{31}P{1H}, ^{13}C{1H} and ^{1}H–^{1}H COSY NMR spectra were recorded on Bruker Avance 400, AMX-400 and JEOL ECZ500R/M3 spectrometers. Mass spectra were recorded on a Bruker maXis II ESI-QTOF instrument in the ESI+ mode. Microanalyses were carried out at the analytical laboratory of the University of Eastern Finland.

Synthesis

General procedure for the preparation of phosphonium salts 1[OTf], **3[OTf], 6[OTf] and 7[OTf]**: Bromoaryl derivative with an amine donor function (1.00 eq.), $NiBr_2$ (0.20 eq.), appropriate tertial phosphine (PPh_3 or PCy_3, 1.05 eq.) and ethylene glycol (3–6 mL) were placed in a 15 mL sealed tube, degassed, and placed under a nitrogen atmosphere. The suspension was stirred for 8 hours at 180 °C until the solution became homogeneous. Then the reaction mixture was cooled down to room temperature and poured into dichloromethane (50 mL). The organic layer was washed with water (3 × 100 mL), dried over anhydrous Na2SO4 for 30 min, filtered through a pad of Celite and evaporated in vacuo. The residue was washed with toluene (3 × 50 mL), diethyl ether (3 × 50 mL), and finally purified by column chromatography (Silica gel 70-230 mesh, ⌀3×20 cm, eluent dichloromethane-methanol, 99:1→92:8 v/v mixture) to afford phosphonium salts as amorphous solids. Bromide salts were subjected to subsequent ion exchange by dissolving them in a saturated DCM solution of potassium trifluoromethanesulfonate. The resulting suspension was filtered through a pad of Celite and evaporated. The crude solid was passed through a Silica column (Silica gel 70-230 mesh, ⌀2.5×5 cm, eluent dichloromethane-methanol, 95:5 v/v mixture).

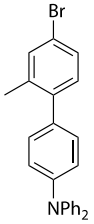

(**a1**) The synthesis was carried out under a nitrogen atmosphere. To a mixture of 4-bromo-1-iodo-2-methylbenzene (1.54 g, 5.20 mmol), [4-(diphenylamino)phenyl]boronic acid (1.50 g, 5.20 mmol), $Pd(PPh_3)_2Cl_2$ (0.07 g, 0.10 mmol) and K_2CO_3 (2.15 g, 15.60 mmol) were added a separately degassed 1,4-dioxane (70 ml) and water (10 ml). The reaction mixture was stirred at 60 °C for 3 h, and after cooled down to room temperature, filtered through Celite and evaporated in vacuo. The obtained pale slurry was extracted by DCM (3 x 50 ml). Combined organic layers were dried over anhydrous Na_2SO_4, filtered, and evaporated in vacuo. The resulting pale-yellow solid was purified by column chromatography (Silica gel 70-230 mesh, 3×15 cm, eluent hexane/DCM, 95/5, v/v) to afford a white powder (1.70 g, 79%). ^{1}H NMR ($CDCl_3$, 298 K; δ): 7.41 (s, –MeC_6H_3–, 1H), 7.35 (d, J = 8.2 Hz, –MeC_6H_3–, 1H), 7.26–7.29 (m, NPh_2, 4H), 7.09–7.15 (m, 9H), 7.04 (t, J = 7.4 Hz, NPh_2, 2H) 2.30 (s, Me, 3H). ^{13}C NMR (CD_2Cl_2, 298 K; δ): 147.78 (s), 146.98 (s), 140.58 (s), 137.79 (s), 134.65 (s), 133.15 (s), 131.45 (s), 129.93 (s), 129.42 (s), 128.92

(s), 124.63 (s), 123.14 (s), 120.86 (s), 20.62 (s).

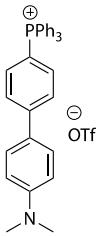

(**1[OTf]**) Prepared from 4'-bromo-*N*,*N*-dimethyl[1,1'-biphenyl]-4-amine (393 mg, 1.43 mmol), triphenylphosphine (394 mg, 1.50 mmol), nickel(II)bromide (63 mg, 0.29 mmol), and 6 ml of ethylene glycol to afford greenish precipitate (590 mg, 68 %). ESI-MS (*m/z*): $[M]^+$ 458.2027 (calcd 458.2033). ^{1}H NMR (CD_2Cl_2, 298 K; *δ*): 7.87–7.91 (m, biph + PPh_3, 5H), 7.73 (td, *J* = 8.0, 3.6 Hz, PPh_3, 6H), 7.55–7.65 (m, PPh_3 + biph, 10H), 6.79 (d, J = 9.0 Hz, biph, 2H), (s, NMe_2, 6H). $^{31}P\{^1H\}$ NMR (CD_2Cl_2, 298 K; *δ*): 23.43 (s, P^+Ph_3, 1P). ^{13}C NMR (CD_2Cl_2, 298 K; *δ*): 151.48 (s), 148.36 (s), 135.63 (s), 134.83 (s), 134.41 (s), 130.63 (s), 128.09 (s), 127.25 (s), 124.49 (s), 118.51 (s), 117.79 (s), 112.45 (s), 40.03 (s). $^{19}F\{^1H\}$ NMR (CD_2Cl_2, 298 K; *δ*): -78.80(s). Anal. Calc. for $C_{33}H_{29}F_3NO_3PS$ Calculated: C, 65.23; H, 4.81; N, 2.31; S, 5.28; Found: C, 65.34; H, 4.98; N, 2.17; S, 5.32.

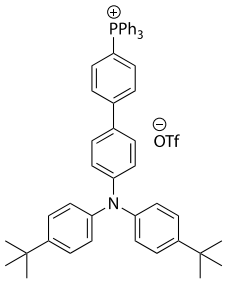

(**3[OTf]**) Prepared from 4'-bromo-*N*,*N*-bis(4-(*tert*-butyl)phenyl)-[1,1'-biphenyl]-4-amine (159 mg, 0.31 mmol), triphenylphosphine (86 mg, 0.33 mmol), nickel(II)bromide (14 mg, 0.06 mmol), and 3 ml of ethylene glycol to afford greenish-orange precipitate (154 mg, 59 %). ESI-MS (*m/z*): $[M]^+$ 694.3596 (calcd 694.3597). ^{1}H NMR (CD_2Cl_2, 298 K; *δ*): 7.83 – 7.97 (m, biph + PPh_3), 7.74 (td, *J* = 7.9, 3.6 Hz, PPh_3, 6H), 7.56–7.64 (m, biph + PPh_3, 8H), 7.31 (d, *J* = 8.5 Hz, NPh_2^{tBu}, 4H), 7.05 (d, *J* = 8.5 Hz, biph+NPh_2^{tBu}, 6H), 1.29 (s, NPh_2^{tBu}, 18H). $^{31}P\{^1H\}$ NMR (CD_2Cl_2, 298 K; *δ*): 23.52 (s, P^+Ph_3, 1P). ^{13}C NMR (CD_2Cl_2, 298 K; *δ*): 149.80 (s), 147.28 (s), 144.23 (s), 135.71 (s), 134.93 (d), 134.46 (d), 130.62 (d), 129.48 (s), 127.95 (s), 127.83 (s), 126.42 (s), 125.10 (s), 121.12 (s), 118.31 (s), 117.59 (s), 31.17 (s). $^{19}F\{^1H\}$ NMR (CD_2Cl_2, 298 K; *δ*): -78.76(s). Anal. Calc. for $C_{51}H_{49}F_3NO_3PS$ Calculated: C, 72.58; H, 5.85; N, 1.66; S, 3.80; Found: C, 72.36; H, 5.91; N, 1.70; S, 3.88.

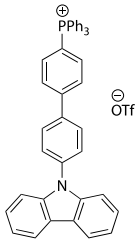

(**4[OTf]**). Potassium trifluoromethanesulfonate (175 mg, 0.92 mmol) was added to a solution of [4'-(9*H*-carbazol-9-yl)[1,1'-biphenyl]-4-yl]triphenyl-phosphoniumbromide (580 mg, 0.88 mmol) in dichloromethane (5 ml). The reaction mixture was stirred at room temperature for 20 min. The resulting suspension was filtered through a pad of Celite and evaporated. The crude yellow solid was purified by column chromatography (Silica gel 70-230 mesh, ⌀2.5×17 cm, eluent dichloromethane-methanol, 99:1 → 95:5 v/v mixture) to afford yellow solid (470 mg, 74 %). ESI-MS (*m/z*): $[M]^+$ 580.2181 (calcd 580.2189). ^{1}H NMR (CD_2Cl_2, 298 K; *δ*): 8.16 (d, J_{HH} 7.9 Hz, 2H, carbazole), 8.07–8.03 (m, 2H, -bph-), 7.9 –7.91 (m, 5H, -Ph + -biph-), 7.8 –7.64 (m, 16H, -PPh3 + -bph-), 7.49 (d, J_{HH} 8.3 Hz, 2H, carbazole), 7.45–7.41 (m, 2H, carbazole), 7.33–7.29 (m, 2H, carbazole). $^{31}P\{^1H\}$ NMR (CD_2Cl_2, 298 K; *δ*): 23.75 (s, P^+Ph_3, 1P). ^{13}C NMR (CD_2Cl_2, 298 K; *δ*): 147.53, 140.59, 138.93, 137.05, 135.82 (d), 135.17 (d), 134.53 (d), 130.71 (d), 129.04 (t), 127.59, 126.16, 123.62, 120.37 (d), 118.06, 117.35, 116.34, 115.62, 109.75. $^{19}F\{^1H\}$ NMR (CD_2Cl_2, 298 K; *δ*): -78.84(s). Anal. Calc. for $C_{43}H_{31}F_3NO_3PS$ Calculated: C, 70.77; H, 4.28; N, 1.92; S, 4.39; Found: C, 70.47; H, 4.39; N, 1.87; S, 4.48.

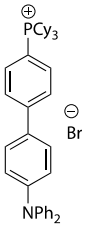

(**5[Br]**) 4-Bromo-4´-(*N,N*-diphenylamino)-biphenyl (200 mg, 0.50 mmol), $NiBr_2$ (22 mg, 0.10 mmol), tricyclohexylphosphine (147 mg, 0.53 mmol) and ethylene glycol (3 mL) were placed in a 10 mL sealed tube, degassed, and placed under a nitrogen atmosphere. The suspension was stirred for 3 hours at 180 °C until the solution became homogeneous. Then the reaction mixture was cooled down to room temperature and poured into dichloromethane (50 mL). The organic layer was washed with water (3 × 100 mL), dried over anhydrous Na2SO4 for 30 min, filtered through a pad of Celite, and evaporated in vacuo. The residue was washed with toluene (3 × 50 mL), diethyl ether (3 × 50 mL), and finally purified by column chromatography (Silica gel 70-230 mesh, ⌀3×20 cm, eluent dichloromethane-methanol, 99:1→92:8 v/v mixture) to afford phosphonium salts **5Br** as amorphous solids (270 mg, 90 %). Recrystallization of **5Br** from methanol-hexane (1-1, v-v) mixture delivers crystals suitable for SC-XRD analysis. ESI-MS (*m/z*): $[M]^+$ 600.3793 (calcd 600.3788). ^1H NMR (CD_2Cl_2, 298 K; *δ*): 7.89 (dd, *J* = 8.5, 2.6 Hz, biph 2H), 7.66 (t, *J* = 8.5 Hz, biph, 2H), 7.53 (d, *J* = 8.6 Hz, biph, 2H), 7.28 (t, *J* = 7.8 Hz, NPh_2, 4H), 7.06–7.12 (m, biph+NPh_2, 8H), 2.79 (br q, *J* = 9.2 Hz, PCy_3, 3H), 1.92–1.96 (m, PCy_3, 12H), 1.80 (d, *J* = 13.2 Hz, PCy_3, 3H), 1.41–1.51 (m, PCy_3, 9H), 1.24–1.28 (m, PCy_3, 3H). $^{31}P\{^1H\}$ NMR (CD_2Cl_2, 298 K; *δ*): 29.89 (s, P^+Cy_3, 1P). ^{13}C NMR (CD_2Cl_2, 298 K; *δ*): 149.04 (s), 147.22 (s), 146.60 (s), 133.42 (d), 131.14 (s), 129.50 (s), 128.13 (s), 128.00(s), 125.18(s), 123.82(s), 122.65(s), 110.32 (s), 109.72 (s), 29.83 (d), 26.74 (s), 26.68 (s), 26.58 (s), 25.52 (s). $^{19}F\{^1H\}$ NMR (CD_2Cl_2, 298 K; *δ*): -78.84(s). Anal. Calc. for $C_{43}H_{51}NPBr$ Calculated: C, 74.10; H, 7.55; N, 2.06; Found: C, 73.98; H, 7.70; N, 2.09.

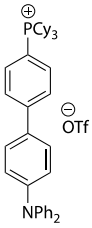

(**5[OTf]**) Prepared according to the procedure described for **4OTf** from **5Br** (240 mg, 0.40 mmol) by metathesis reaction with potassium trifluoromethanesulfonate (yield 92%). ESI-MS (*m/z*): $[M]^+$ 600.3794 (calcd 600.3788). ^1H NMR (CD_2Cl_2, 298 K; *δ*): 7.89 (dd, *J* = 8.5, 2.6 Hz, biph 2H), 7.66 (t, *J* = 8.5 Hz, biph, 2H), 7.53 (d, *J* = 8.5 Hz, biph, 2H), 7.28 (t, *J* = 7.8 Hz, NPh_2, 4H), 7.06–7.12 (m, biph+NPh_2, 8H), 2.79 (br q, *J* = 9.2 Hz, PCy_3, 3H), 1.92–1.96 (m, PCy_3, 12H), 1.80 (d, *J* = 13.2 Hz, PCy_3, 3H), 1.41–1.51 (m, PCy_3, 9H), 1.24–1.28 (m, PCy_3, 3H). $^{31}P\{^1H\}$ NMR (CD_2Cl_2, 298 K; *δ*): 29.89 (s, P^+Cy_3, 1P). ^{13}C NMR (CD_2Cl_2, 298 K; *δ*): 149.04 (s), 147.22 (s), 146.60 (s), 133.42 (d), 131.14 (s), 129.50 (s), 128.13 (s), 128.00(s), 125.18(s), 123.82(s), 122.65(s), 110.32 (s), 109.72 (s), 29.83 (d), 26.74 (s), 26.68 (s), 26.58 (s), 25.52 (s). $^{19}F\{^1H\}$ NMR (CD_2Cl_2, 298 K; *δ*): -78.84(s). Anal. Calc. for $C_{43}H_{51}F_3NO_3PS$ Calculated: C, 68.87; H, 6.86; N, 1.87; S, 4.28; Found: C, 68.99; H, 6.71; N, 1.69; S, 4.11.

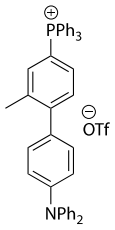

(**6[OTf]**) Prepared from 7-bromo-9,10-dihydro-*N*,*N*-diphenyl-2-phenanthrenamine (223 mg, 0.54 mmol), triphenylphosphine (149 mg, 0.57 mmol), nickel(II)bromide (24 mg, 0.11 mmol), and 3 ml of ethylene glycol to afford yellow solid (257 mg, 80 %). ESI-MS (*m/z*): $[M]^+$ 596.2508 (calcd 596.2502). ^1H NMR (CD_2Cl_2, 298 K; *δ*): 7.91 (t, *J* = 7.2 Hz, PPh_3, 3H), 7.76 (td, *J* = 7.9, 3.5 Hz, PPh_3, 6H), 7.65 (dd, *J* = 12.9, 7.6 Hz, biph+PPh_3, 6H), 7.57 (dd, *J* = 7.7, 3.8 Hz, biph, 1H), 7.43 (t, *J* = 11.0 Hz, biph, 2H), 7.19–7.34 (m, NPh_2+biph, 6H), 7.00–7.17 (m, NPh_2+biph, 8H), 2.38 (s, Me, 3H). $^{31}P\{^1H\}$ NMR (CD_2Cl_2, 298 K; *δ*): 23.48 (s, P^+Ph_3, 1P). ^{13}C NMR (CD_2Cl_2, 298 K; *δ*): 149.26 (s), 148.13 (s), 147.42 (s), 138.76 (d), 136.06 (s), 135.98 (s), 134.52 (d), 129.77 (s), 129.47 (s), 125.00 (s), 123.60 (s), 122.38 (s), 118.30

(s), 117.59 (s), 115.39 (s), 114.67 (s), 20.89 (s). $^{19}F\{^{1}H\}$ NMR (CD_2Cl_2, 298 K; δ): -78.60 (s). Anal. Calc. for $C_{44}H_{35}F_3NO_3PS$ Calculated: C, 70.86; H, 4.73; N, 1.88; S, 4.30; Found: C, 70.99; H, 4.70; N, 1.71; S, 4.80.

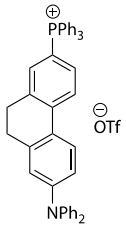

(**7[OTf]**). Prepared from 7-Bromo-9,10-dihydro-*N*,*N*-diphenyl-2-phenanthrenamine (420 mg, 0.99 mmol), triphenylphosphine (270 mg, 1.0 mmol), nickel(II)bromide (43 mg, 0.20 mmol), and 6 ml of ethylene glycol to afford yellow solid (480 mg, 71 %). ESI-MS (*m/z*): $[M]^+$ 608.2497 (calcd 608.2502). ^{1}H NMR (CD_2Cl_2, 298 K; δ): 7.94–7.87 (m, 4H, $-P^+Ph_3$ + $-C_6H_3-$), 7.77–7.71 (td, J_{HH} 7.8 Hz, 3.5 Hz, 6H, $-P^+Ph_3$), 7.67–7.59 (m, 7H, $-P^+Ph_3$ + $-C_6H_3-$), 7.42 (ddd, J_{HH} 12.7 Hz, 8.1 Hz, 1.9 Hz, 1H, $-C_6H_3-$), 7.36–7.27 (m, 5H, $-NPh_2$ + $-C_6H_3-$), 7.14–7.08 (m, 6H, $-NPh_2$), 6.96 (dd, J_{HH} 8.6 Hz, 2.5 Hz, 1H, $-C_6H_3-$), 6.90 (d, J_{HH} 2.4 Hz, 1H, $-C_6H_3-$), 2.88–2.82 (m, 2H, $-CH_2-CH_2-$), 2.80–2.74 (m, 2H, $-CH_2-CH_2-$). $^{31}P\{^{1}H\}$ NMR (CD_2Cl_2, 298 K; δ): 23.34 (s, P^+Ph_3, 1P). ^{13}C NMR (CD_2Cl_2, 298 K; δ): 149.63, 147.02, 142.10, 139.66, 138.98 (d), 135.61 (d), 134.45 (d), 133.34 (dd), 130.57 (d), 129.52, 125.81, 125.47, 125.15, 124.49 (d), 124.05, 120.94, 120.61, 118.52, 117.81, 113.25, 112.51, 28.96, 28.45. $^{19}F\{^{1}H\}$ NMR (CD_2Cl_2, 298 K; δ): –78.88 (s). Anal. Calc. for $C_{45}H_{35}F_3NO_3PS$ Calculated: C, 71.32; H, 4.66; N, 1.85; S, 4.23; Found: C, 72.47; H, 4.97; N, 1.85; S, 2.81.

X-ray single-crystal structure determination

The crystal of **5[Br]** was immersed in a film of NVH oil, mounted on a polyimide microloop (MicroMounts of MiTeGen), transferred to a stream of cold nitrogen (Bruker Kryoflex2), and measured at a temperature of 150K. The X-ray diffraction data were collected on a Bruker D8 Venture diffractometer with a CMOS Photon 100 and multilayer optics monochromated MoKα (0.71073 Å) radiation (INCOATEC microfocus sealed tube). The frames were integrated with the Bruker SAINT software package using a narrow-frame algorithm. The APEX3 v2018.7-0 program package was used for cell refinements and data reductions. The structure was solved using intrinsic phasing method[7,8], refined and visualized with the OLEX2-1.3 and Diamond-4.6.4 programs. A semiempirical absorption correction (SADABS) was applied to all data. All non-hydrogen atoms were refined anisotropically. Hydrogen atoms were included in structure factors calculations. All Hydrogen atoms were assigned to idealized geometric positions.

Table S1 Crystal data and structure refinement parameters for **5[Br]**.

Identification code	**5[Br]**
CCDC number	**2366427**
Empirical formula	$C_{43}H_{55}BrNOP$
Formula weight	712.76
Temperature/K	150
Crystal system	monoclinic
Space group	C2/c
a/Å	43.754(11)
b/Å	9.850(3)
c/Å	17.372(5)
α/°	90
β/°	95.708(16)
γ/°	90
Volume/Å^3	7450(3)
Z	8
ρ_{calc}g/cm^3	1.271
μ/mm^{-1}	1.180
F(000)	3024.0
Crystal size/mm^3	0.21 × 0.11 × 0.09
Radiation	MoKα (λ = 0.71073)
2Θ range for data collection/°	1.87 to 51.998
Index ranges	-53 ≤ h ≤ 52, -12 ≤ k ≤ 12, -18 ≤ l ≤ 21
Reflections collected	25695
Independent reflections	7149 [R_{int} = 0.0725, R_{sigma} = 0.0863]
Data/restraints/parameters	7149/0/426
Goodness-of-fit on F^2	0.986
Final R indexes [I>=2σ (I)]	R_1 = 0.0450, wR_2 = 0.0843
Final R indexes [all data]	R_1 = 0.0867, wR_2 = 0.0962
Largest diff. peak/hole / e Å^{-3}	0.70/-0.38

[a] $R_1 = \sum||F_o|-|F_c||/\sum|F_o|$; $wR_2 = [\sum[w(F_o^2-F_c^2)^2/\sum[(wF_o^2)^2]]^{1/2}$; $w = 1/[\sigma^2(F_o^2)+(aP)^2+bP]$, where $P = (F_o^2+2F_c^2)/3$

[b] GooF = $S = [[\sum w(F_o^2-F_c^2)^2]/(m-n)]^{1/2}$, where m = number of reflexes and n = number of parameters

2.Steady-state measurements

Steady-state absorption spectra were measured by a UH-5700 (Hitachi) absorbance meter. The light source was a deuterium lamp with a wavelength of 200~340nm and a xenon lamp with a wavelength of 340~900nm. We prepared two clean cuvettes (light path 1 cm) containing the same solvent and placed them into the reference holder and the sample holder. We then calibrated the system using the above settings and ensured that the baseline noise was below 2×10^{-3} before measurement. In addition, the absorbance of the sample was kept around 0.1 to avoid the inner filter effect. (Purity examination results are shown in Fig. S1)

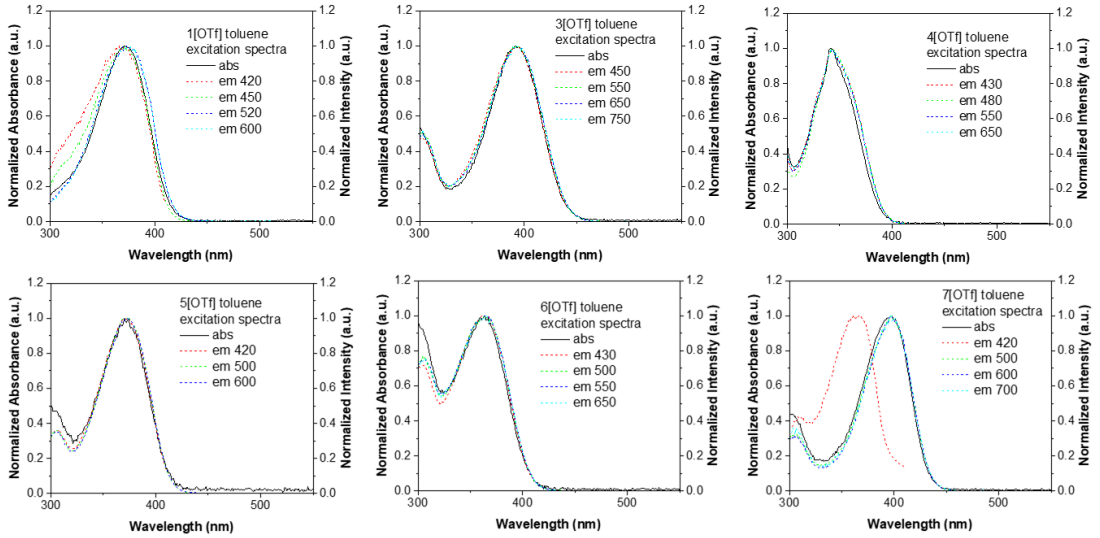

Fig. S1 Excitation spectra of the salts in toluene. **1[OTf]** and **7[OTf]** are excited with 415 nm and 400 nm respectively to avoid interference from impurities.

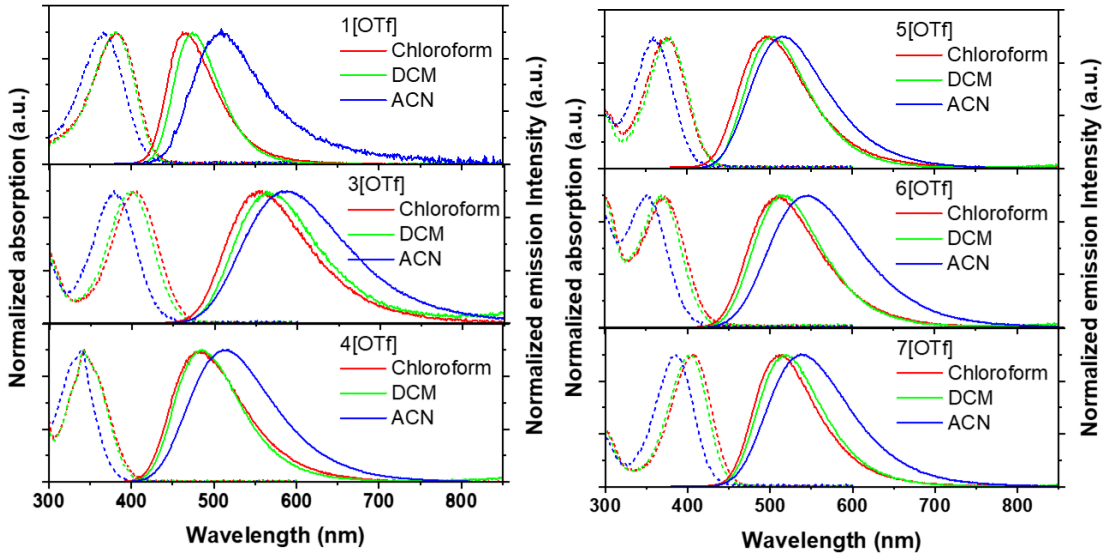

Fig. S2 The steady-state spectra of the salts in polar solvents. Absorption spectra are dash line and emission spectra are solid line.

Table S2. Steady-state properties of **1[OTf]-7[OTf]** in polar solvents.

	solvent	λ_{abs} (nm)	λ_{em} (nm)	Stokes shift (cm^{-1})	PLQY
1[OTf]	chloroform	382	462	4533	0.73
	DCM	380	474	5219	0.54
	ACN	366	509	7676	0.05
3[OTf]	chloroform	405	553	6608	0.51
	DCM	398	563	7364	0.36
	ACN	378	587	9419	0.19
4[OTf]	chloroform	343	483	8451	0.74
	DCM	342	486	8664	0.78
	ACN	339	510	9891	0.54
5[OTf]	chloroform	374	500	6738	0.82
	DCM	375	506	6904	0.78
	ACN	359	514	8400	0.68
6[OTf]	chloroform	373	513	7316	0.70
	DCM	368	517	7832	0.72
	ACN	350	547	10290	0.46
7[OTf]	chloroform	407	511	5001	0.73
	DCM	402	516	5496	0.74
	ACN	386	540	7388	0.57

Steady-state emission and excitation spectra were measured by an FLS980 (Edinburgh) fluorometer. The light source was a Xenon arc lamp, and the detector was a visible light PMT (R928P, Hamamatsu Photonics) which was suitable to the wavelength range 200 ~ 900 nm. The output emission spectrum has been corrected according to an emission correction file to eliminate wavelength-dependent responses of the detector. The excitation correction was performed by dividing the emission signal with the excitation signals from the reference detector after the excitation monochromator. The photoluminescence quantum yield (PLQY) of the sample was compared with the standard coumarin 480 in methanol (Φ = 87%[9]) and was obtained by the following formula[10]

$$\frac{\Phi_S}{\Phi_R} = \frac{OD_R \times F_s \times n_S^2}{OD_S \times F_R \times n_R^2}$$

where the subscripts S and R represent sample and reference, while Φ, OD, F, and n stand for PLQY, the absorbance at excitation wavelength, integral of emission spectra, refractive index.

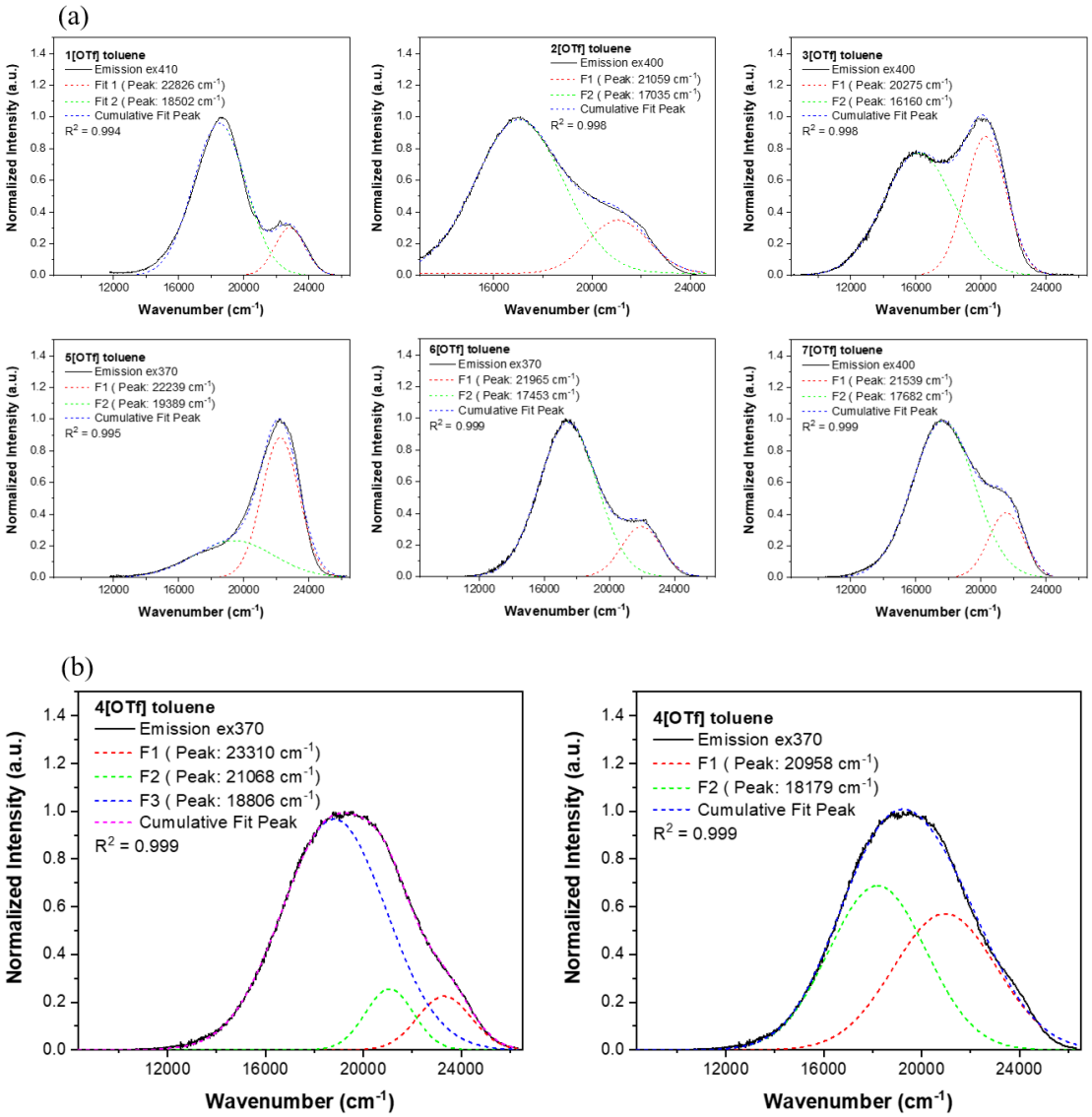

Fig. S3 (a) Fitting data of the emission spectra in the toluene except **4[OTf]**. (b) **4[OTf]** is fitted with three and two Gaussian functions, and the former is more reasonable because an emission peak at about 23224 cm^{-1} was observed in the TRES results (183.12 ps).

Toluene, chloroform, dichloromethane (DCM), and acetonitrile (ACN) were solvents for UV/vis spectroscopy (Merck). The purity of ethylbenzene, cumene, n-propylbenzene, and sec-butylbenzene was 98 ~ 99 % and the impurities in solvents did not affect our spectroscopic measurements (Fig. S4).

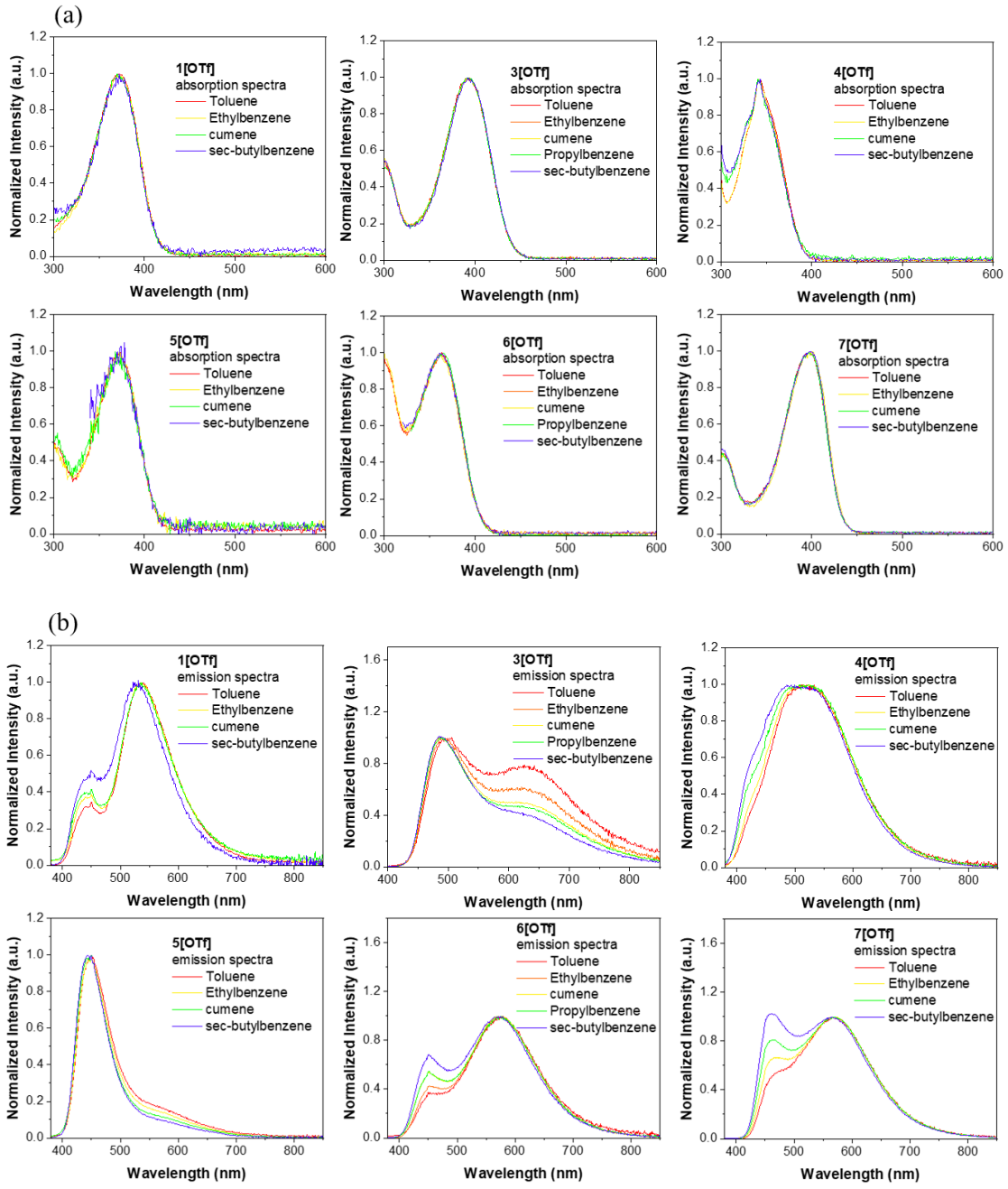

Fig. S4 Steady-state measurement in the weakly polar solvents (toluene, ethylbenzene, cumene, n-propylbenzene, sec-butylbenzene). (a) exhibits the absorption spectra, while (b) exhibits the emission spectra.

3.Time-resolved measurements

The time-correlated single photon counting (TCSPC) technique was employed for picosecond to nanosecond lifetime measurements using the OB-900L lifetime spectrometer from Edinburgh. The excitation pulse was generated by second harmonic generation (SHG) of an 82 MHz femtosecond Ti:Sapphire-based oscillator (Spectra-Physics) and we tuned the pulse repetition rate by the pulse picker (model 3980, Spectra-Physics). Sample fluorescence was collected perpendicular to the excitation light path. A half-wave plate, which was set as 54.7° (magic angle) relative to the excitation pulse polarization, was placed between the sample and the detector. The delayed time of fluorescence was recorded using a time-to-amplitude converter (TAC), with the residual fundamental frequency (FF) and the sample fluorescence serving as the start and stop signals, respectively. To enhance temporal resolution, we integrated the TCSPC system with a multichannel plate (MCP), replacing the regular photomultiplier, thereby reducing the temporal resolution to 15~20 ps.

Table S3 Lifetime information of **1[OTf]** in the weakly polar solvents

1[OTf]	τ at 460 nm (ps)	τ at 650 nm (ps)
Toluene	46.90 (0.84) 336.7 (0.16)	82.94 (-0.40) 1035 (0.60)
Ethylbenzene	34.46 (0.81) 296.2 (0.19)	80.91 (-0.43) 1014 (0.57)
Cumene	45.29 (0.87) 442.4 (0.13)	73.02 (-0.50) 1022 (0.50)
Sec-butylbenzene	34.93 (0.85) 354.2 (0.15)	81.84 (-0.46) 1144 (0.54)

Table S4 Lifetime information of **3[OTf]** in the weakly polar solvents

3[OTf]	τ at 450 nm (ps)	τ at 700 nm (ps)
Toluene	42.38 (0.70) 567.1 (0.30)	403.9 (-0.47) 1569 (0.53)
Ethylbenzene	46.30 (0.72) 653.4 (0.28)	394.8 (-0.47) 1618 (0.53)
Cumene	51.12 (0.72) 762.2 (0.28)	435.7 (-0.47) 1643 (0.53)
N-propylbenzene	49.58 (0.73) 783.2 (0.27)	461.2 (-0.47) 1615 (0.53)
Sec-butylbenzene	56.13 (0.74) 945.3 (0.26)	499.2 (-0.47) 1876 (0.53)

Table S5 Lifetime information of **4[OTf]** in the weakly polar solvents

4[OTf]	τ at 440 nm (ps)	τ at 680 nm (ps)
Toluene	69.23 (0.60) 560.5 (0.37) 4900 (0.03)	495.5 (-0.41) 5918 (0.59)
Ethylbenzene	63.82 (0.59) 550.9 (0.38) 5083 (0.03)	504.5 (-0.41) 5934 (0.59)
Cumene	88.78 (0.62) 688.2 (0.35) 4776 (0.03)	490.6 (-0.41) 6137 (0.59)
Sec-butylbenzene	122 (0.61) 876.7 (0.36) 5323 (0.03)	590.1 (-0.39) 6375 (0.61)

Table S6 Lifetime information of **5[OTf]** in the weakly polar solvents

5[OTf]	τ at 440 nm (ps)	τ at 650 nm (ps)
Toluene	883 (0.64) 3000 (0.36)	930.8 (-0.49) 3415 (0.51)
Ethylbenzene	995.2 (0.63) 3111 (0.37)	1028 (-0.48) 3430 (0.52)
Cumene	1118 (0.66) 3101 (0.34)	1220 (-0.47) 3548 (0.53)
Sec-butylbenzene	1273 (0.64) 2984 (0.36)	1389 (-0.47) 3735 (0.53)

Table S7 Lifetime information of **6[OTf]** in the weakly polar solvents

6[OTf]	τ at 440 nm (ps)	τ at 680 nm (ps)
Toluene	66.08 (0.54) 398.4 (0.46)	299.7 (-0.46) 4272 (0.54)
Ethylbenzene	91.33 (0.53) 484.1 (0.47)	338.4 (-0.47) 4199 (0.53)
Cumene	94.99 (0.58) 582.7 (0.42)	362.3 (-0.46) 4280 (0.54)
N-propylbenzene	112.85 (0.57) 620.0 (0.43)	392.2 (-0.46) 4337 (0.54)
Sec-butylbenzene	114.1 (0.58) 741.0 (0.42)	464.5 (-0.47) 4431 (0.53)

Table S8 Lifetime information of **7[OTf]** in the weakly polar solvents

7[OTf]	τ at 440 nm (ps)	τ at 680 nm (ps)
Toluene	384.1 (0.96) 2944 (0.04)	436.2 (-0.49) 3851 (0.51)
Ethylbenzene	408.4 (0.97) 2603 (0.03)	441.2 (-0.49) 3937 (0.51)
Cumene	467.8 (0.95) 2012 (0.05)	525.1 (-0.48) 3981 (0.52)
Sec-butylbenzene	445.1 (~0.99)	663.4 (-0.48) 4052 (0.52)

Time-resolved emission spectra (TRES)[11] in weakly polar solvents were calculated by

$$I'(\lambda,t)=\frac{F(\lambda)\times I(\lambda,t)}{\int_0^\infty I(\lambda,t)dt}$$

$I(\lambda,t)$ is the emission intensity decay at different wavelengths from TCSPC measurements, $F(\lambda)$ is the steady-state emission intensity at certain wavelength, and $I'(\lambda,t)$ is the result. By substituting the specific time into $I'(\lambda,t)$, the emission spectrum at this moment can be obtained. Next, we normalized each area of TRES to a constant value. Note that, since we cannot obtain TRES over the complete spectral wavelength range, we calculated the area of each spectrum according to Gaussian function fitting. In this way, all spectra would possess equal areas. If the reaction is strictly a two-state process, we would observe a distinct iso-emissive point.[11] Our results (Fig. 2(a) and S5(a)) confirm that anion migration involves multiple emitting species. In order to obtain the time evolution of the Stokes shift of the long-wavelength emission peak and calculate the spectral response function $C(t)$ of anion migration, we selected the time-dependent emission spectrum after 100 ps and fitted it with two Gaussian functions (single Gaussian function fitting for **4[OTf]**). The gradually red-shifted emission peaks are taken as $\nu(t)$. The $\nu(\infty)$ value is given by the longest wavelength emission peak from steady-state measurement or the minimum value of $\nu(t)$. Consequently, we restrict the $C(t)$ value between 0 and 1. After removing the deviation points, the $C(t)$ is fitted with a single exponential function. Noteworthy, we believe excited-state intramolecular charge transfer is no longer significant after 100 ps, so the only factor to influence the charge transfer state of solute is anion, i.e., anion migration occurs after completion of ESICT. As for the solvent relaxation of **3[OTf]** in DCM, we select the TRES around 1 ps as the starting point and the remaining fitting process is the same as **4[OTf]** in toluene.

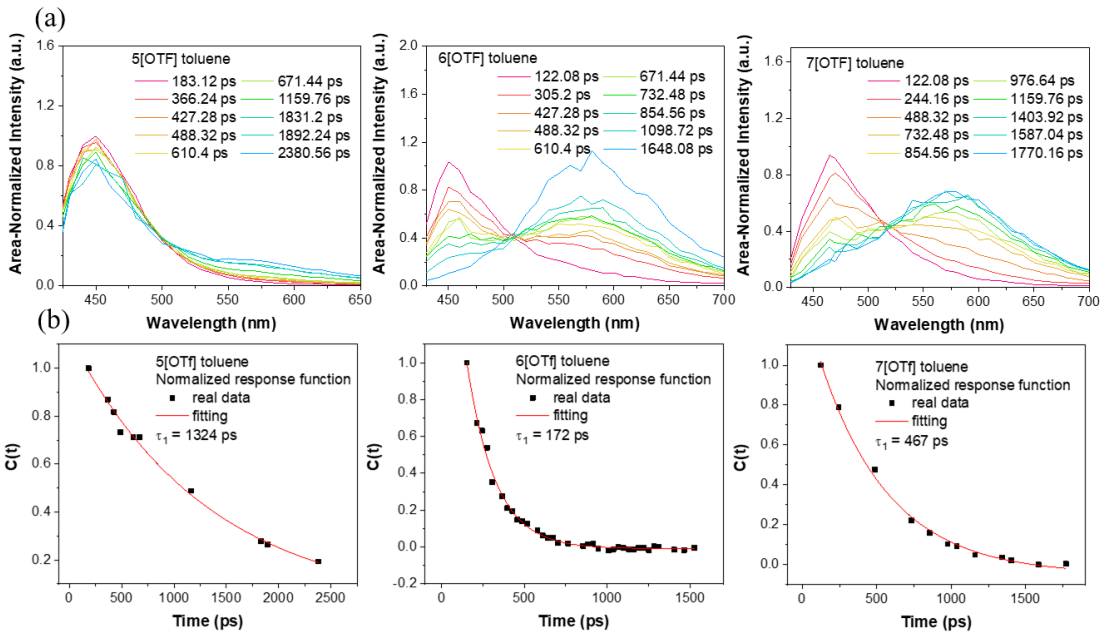

Fig. S5 (a) The TRES of **5[OTf]**, **6[OTf]**, and **7[OTf].** We normalized the area of each spectrum to the same value.[11] (b)The spectral response functions $C(t)$ of **5[OTf]**, **6[OTf]**, and **7[OTf]**.

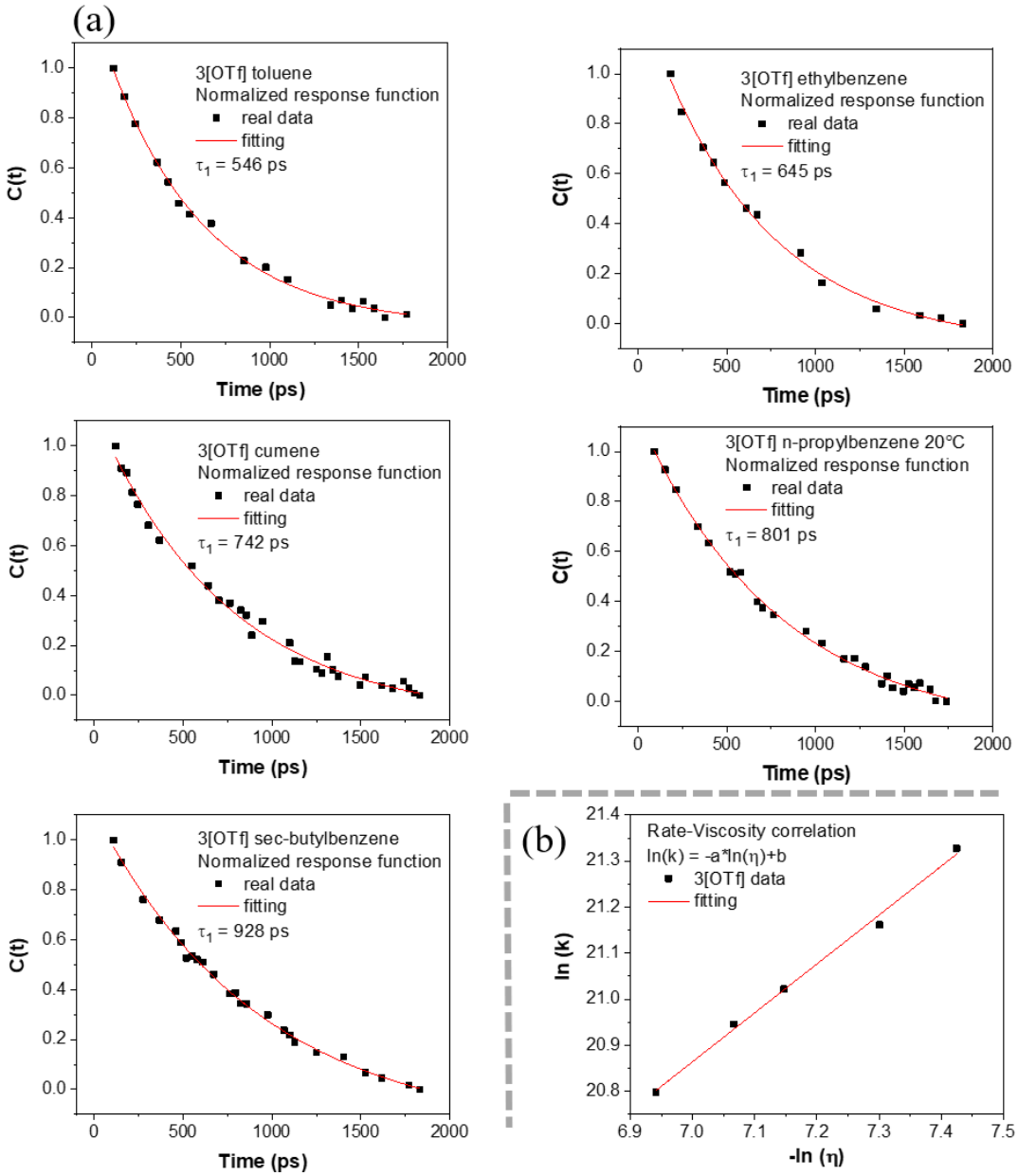

Fig. S6 Details of translocation rate fitting and relationship between translocation rate of **3[OTf]** and viscosity. (a) shows the fitting of C(t) and (b) shows the rate-viscosity correlation of **3[OTf]**.

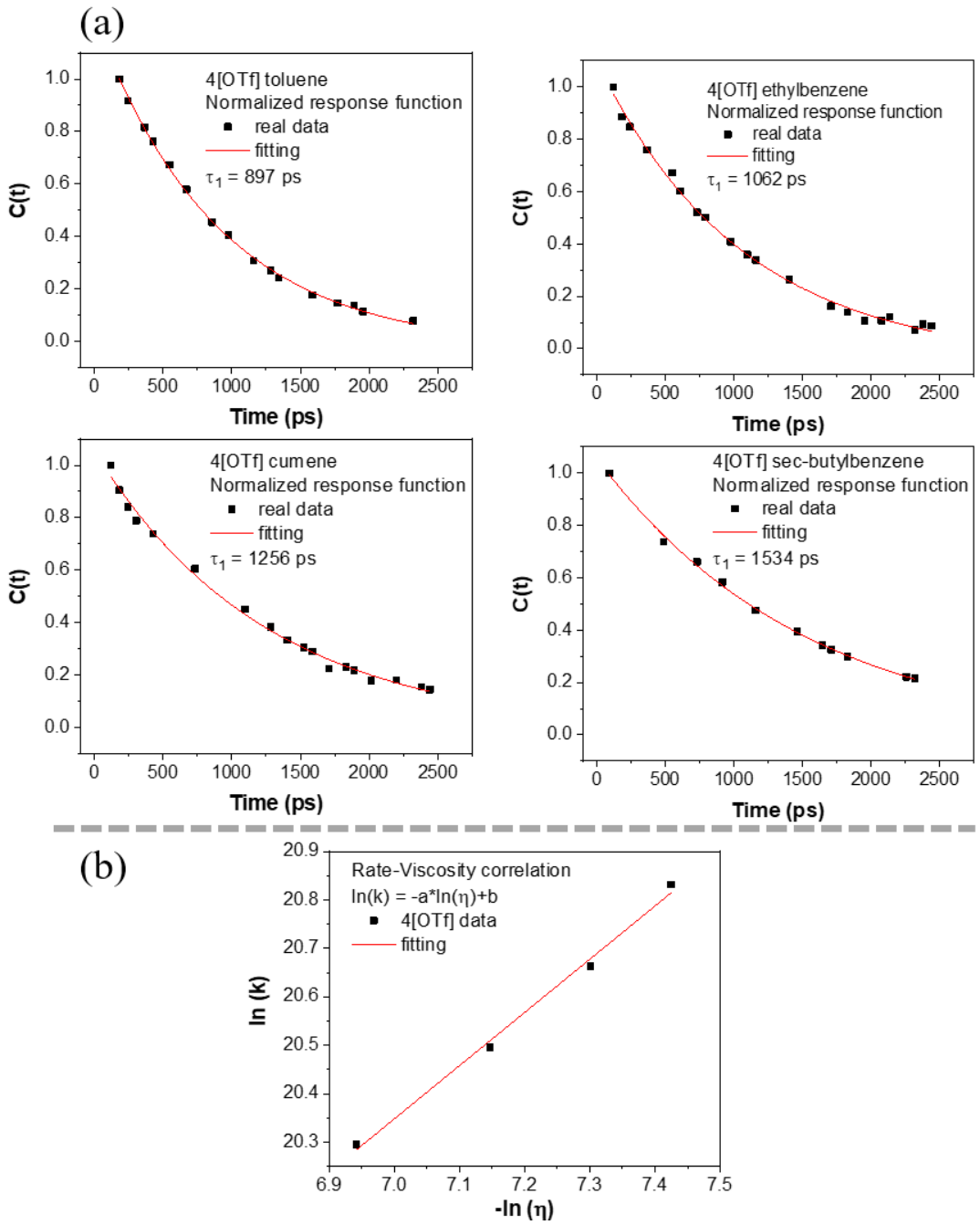

Fig. S7 Details of translocation rate fitting and relationship between translocation rate of **4[OTf]** and viscosity. (a) shows the fitting of C(t) and (b) shows the rate-viscosity correlation of **4[OTf]**.

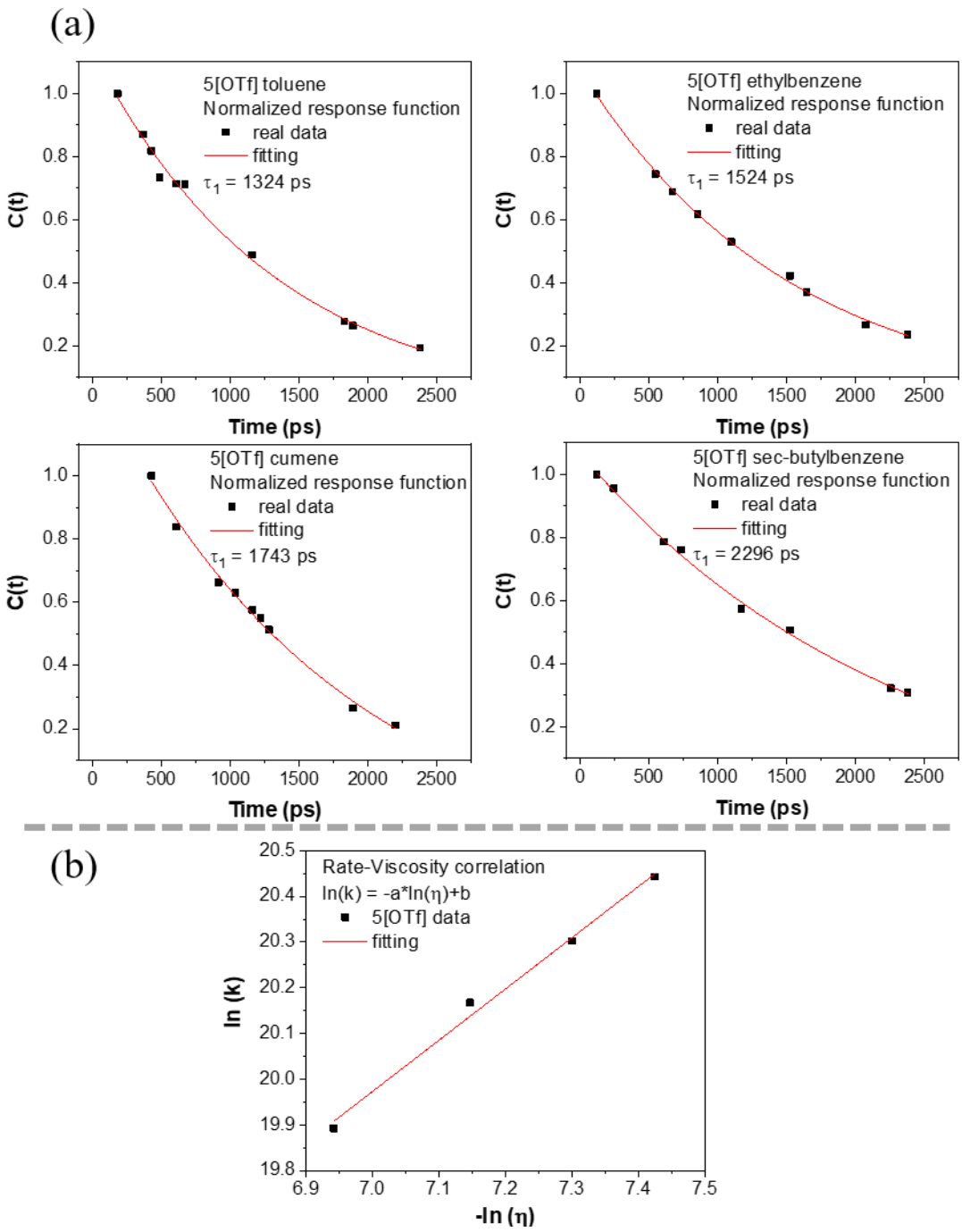

Fig. S8 Details of translocation rate fitting and relationship between translocation rate of **5[OTf]** and viscosity. (a) shows the fitting of C(t) and (b) shows the rate-viscosity correlation of **5[OTf]**.

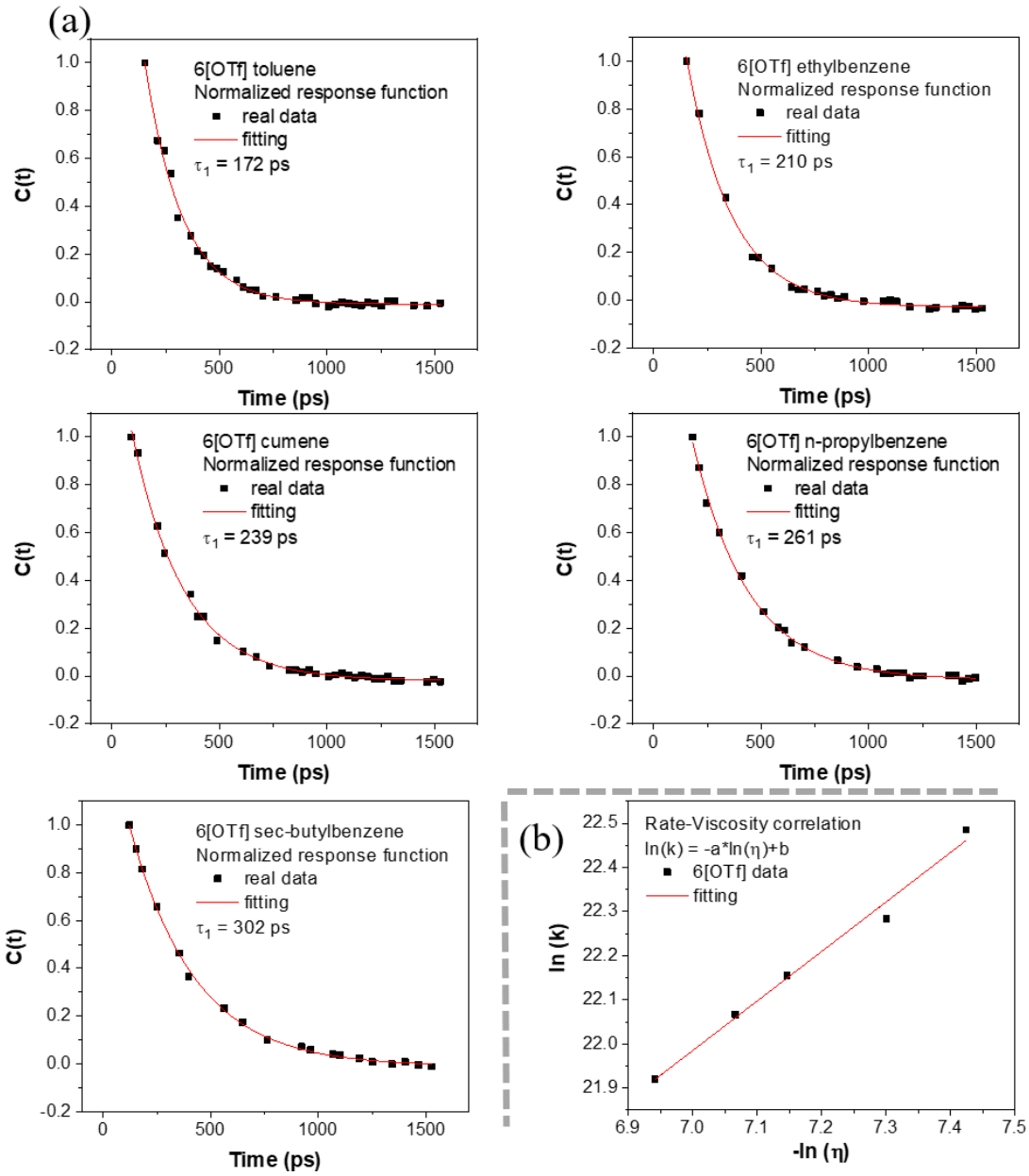

Fig. S9 Details of translocation rate fitting and relationship between translocation rate of **6[OTf]** and viscosity. (a) shows the fitting of C(t) and (b) shows the rate-viscosity correlation of **6[OTf]**.

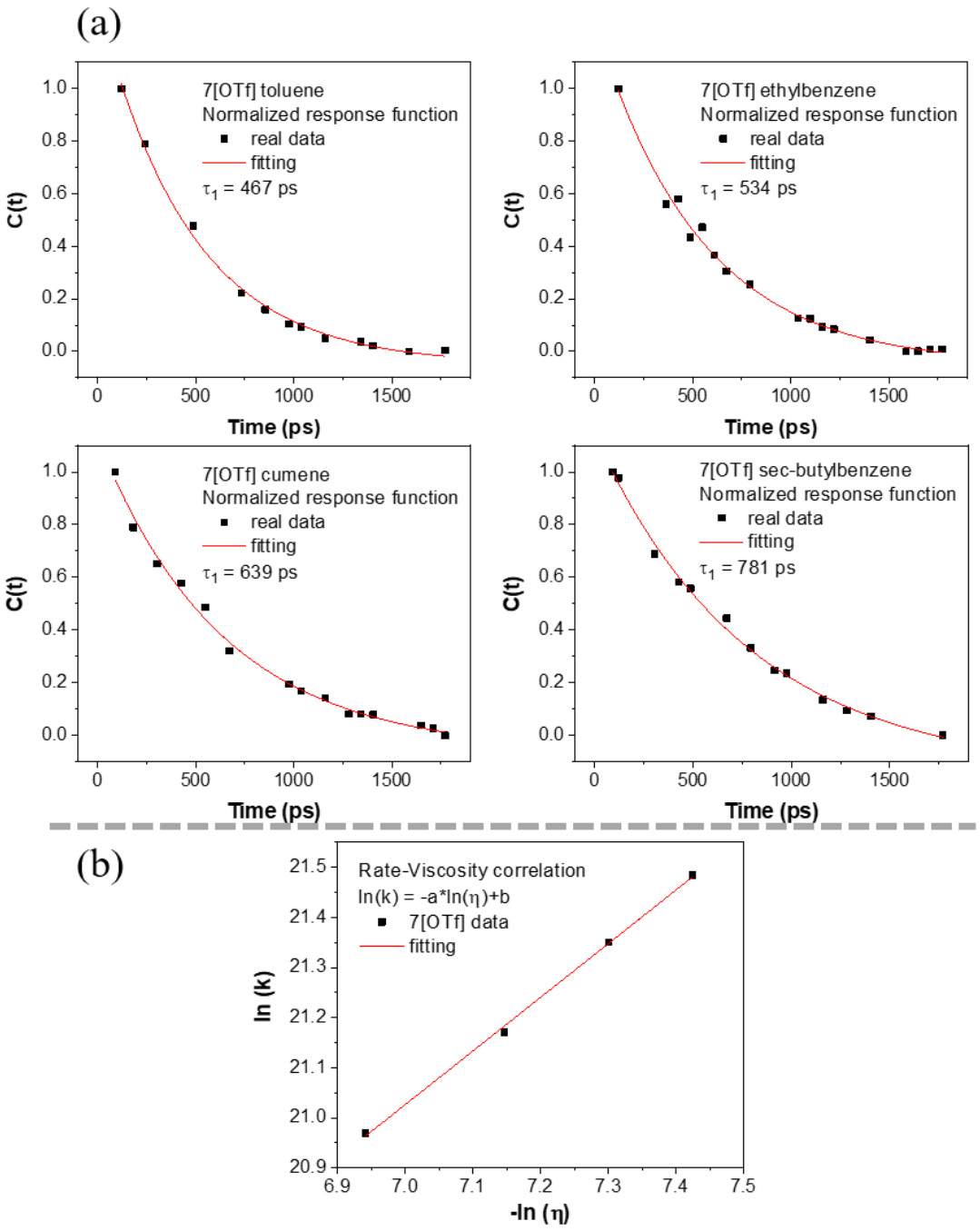

Fig. S10 Details of translocation rate fitting and relationship between translocation rate of **7[OTf]** and viscosity. (a) shows the fitting of C(t) and (b) shows the rate-viscosity correlation of **7[OTf]**.

Temperature-dependent lifetime measurements were conducted using temperature controller and variable temperature cell holder from Specac. To maintain the viscosity of the environment, we utilized toluene, ethylbenzene, cumene, n-propylbenzene, and sec-butylbenzene at different temperatures. (Table S9)[12] Viscosity-dependent lifetime measurements were also performed in the same pure solvents but at the constant temperature (20~21°C, room temperature).

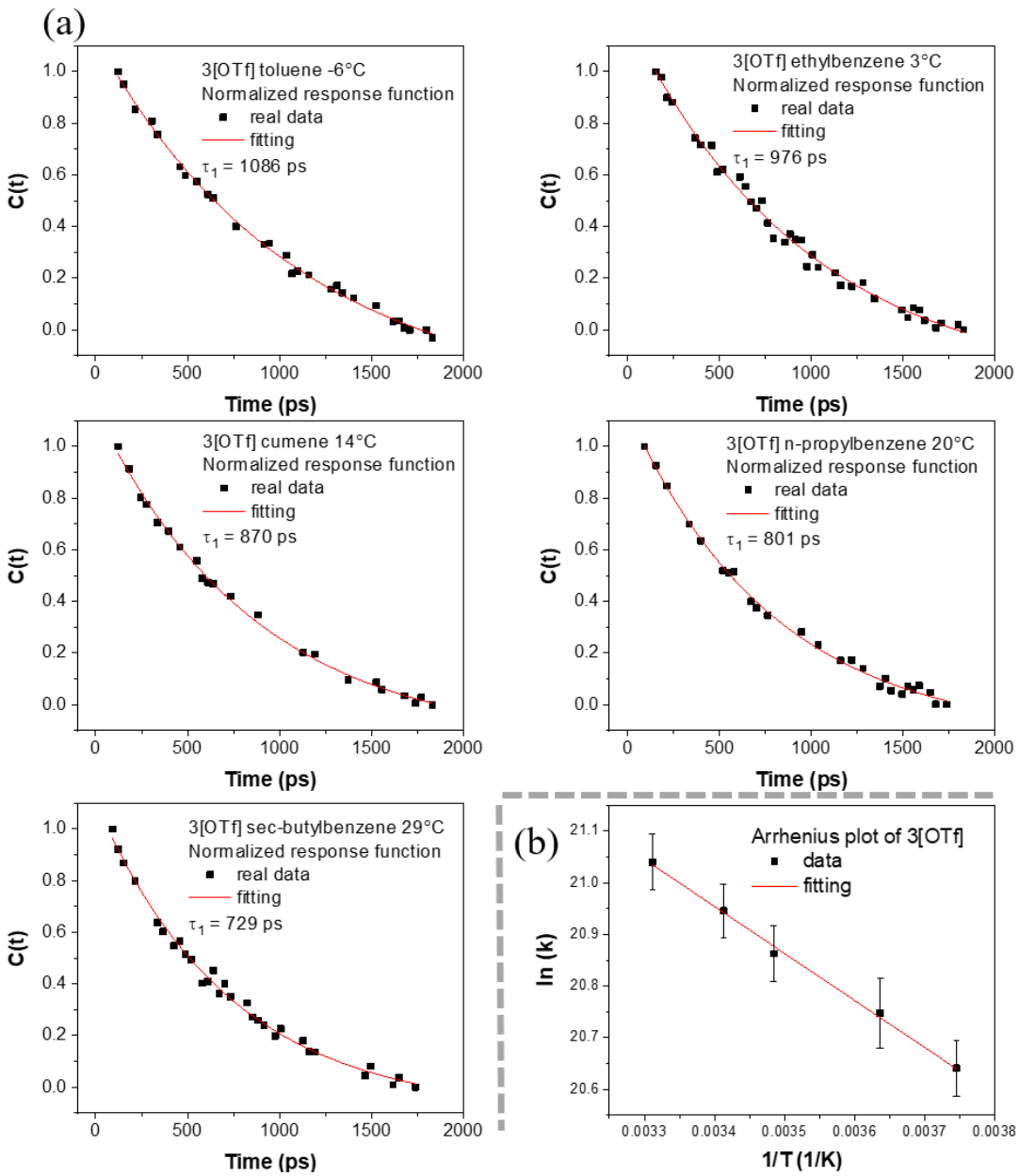

Fig. S11 Translocation rate fitting details of **3[OTf]** at different temperatures and solvents to maintain invariable viscosity: (a) shows the fitting of C(t) at different temperatures and (b) shows the Arrhenius plot of **3[OTf]**.

Table S9 Viscosity of weakly polar solvents at different temperatures.[12]

	Temperature (K)	Viscosity (cP)
Toluene	294.15	0.5964
	267.15	0.8487
Ethylbenzene	294.15	0.6751
	276.15	0.8417
Cumene	294.15	0.7877
	287.15	0.8637
n-propylbenzene	294.15	0.8417
	293.15	0.8534
sec-butylbnezene	294.15	0.9669
	302.15	0.8611

We study the solvent relaxation dynamics of **3[OTf]** in DCM by FOG 100 up-conversion setup (CDP). The light source is produced by a Ti:Sapphire seed laser (Element 2, Spectra-Physics) coupled with a regeneration amplifier (Spifire Ace, Spectra-Physics) with a wavelength 800 nm and a frequency 1 kHz. Using the same method as TCSPC to obtain the excitation pulse 400 nm and gate pulse 800 nm. These two pulses are split into two different light paths, and we again use half-wave plate to set the polarization angle between these two pulses at magic angle. The excitation pulse travels through a rotating cell and generates the fluorescence. While the gate pulse is controlled by a retroreflector coupled to a delay stage and determines the delay time with respect to the excitation pulse. A BBO crystal is used for sum frequency generation of the focused fluorescence signal and the gate pulse. The experimental full width at half maximum (FWHM) of instrument response function (IRF) is about 90 fs, determined from Raman scattering. By fitting the intensity variations of the sum-frequency signals at different delay times with a given IRF, lifetime information at specific wavelength can be obtained.

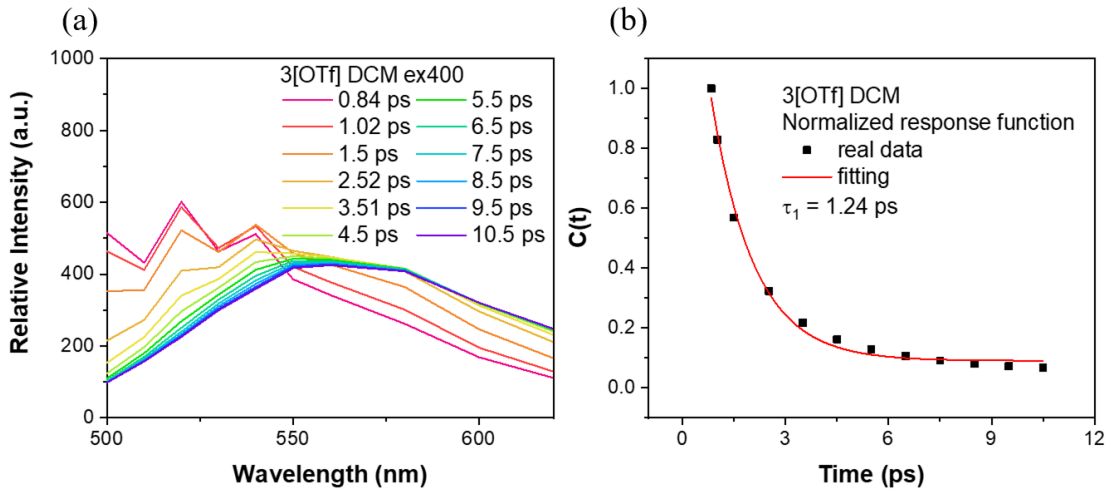

Fig. S12 (a) The TRES of **3[OTf]** in dichloromethane (DCM) without normalization. (b) The spectral response function C(t) of **3[OTf]**. The time-resolved emission peaks were fitted with a single Gaussian function at each TRES and the result shows a typical single-exponential decay.

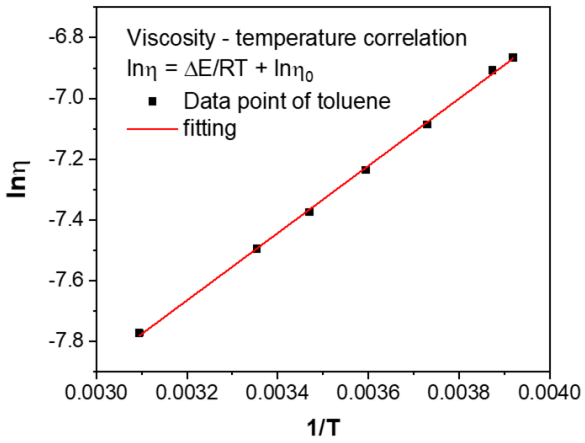

Fig. S13 (a) Viscosity-temperature correlation of toluene.[13] ($\Delta E = 2.19\ kcal/mol$ and $\eta_0 = 0.013\ mPa \cdot s$) The ΔE is activation energy of the diffusion in the viscous liquid, while η_0 is called pre-exponential factor or entropic factor is related to viscosity under gas phase.[14,15]

4.Computational information

Computation study on phosphonium cations was performed by the Gaussian 16 package[16]. The structural optimization of ground state (S_0) were calculated by the density functional theory (DFT) at M06-2X/6-31+G(d,p)[17,18] level with a polarizable continuum model (PCM)[19] in toluene solvents. And the time-dependent density functional theory (TDDFT) calculations for transition energies and optimized structures in the lowest singlet excited state (S_1') were carried out with the same functional and basis set. The output results from DFT/TDDFT calculations were subsequently employed in the Multiwfn[20] program to complete the following calculations.

Hole-electron distribution[21] of cation was analyzed by Multiwfn. We used the optimized ground state structure to calculate the hole-electron distribution for the $S_0 \rightarrow S_1$, while the $S_0' \rightarrow S_1'$ transition was calculated using the optimized excited state structure. The definitions and indices for investigating charge transfer characteristics of cations are introduced below and details can refer to the manual of Multiwfn.

First, $\rho^{hole}(\boldsymbol{r})$ and $\rho^{elec}(\boldsymbol{r})$ indicate the density distribution of hole and electron. They are defined as:

$$\rho^{hole}(\boldsymbol{r}) = \sum_{i}^{occ}\sum_{a}^{vir}(w_i^a)^2\varphi_i(\boldsymbol{r})\varphi_i(\boldsymbol{r}) + \sum_{i}^{occ}\sum_{j\neq i}^{occ}\sum_{a}^{vir} w_i^a w_j^a \varphi_i(\boldsymbol{r})\varphi_j(\boldsymbol{r})$$

$$\rho^{elec}(\boldsymbol{r}) = \sum_{i}^{occ}\sum_{a}^{vir}(w_i^a)^2\varphi_a(\boldsymbol{r})\varphi_a(\boldsymbol{r}) + \sum_{i}^{occ}\sum_{a}^{vir}\sum_{a\neq b}^{vir} w_i^a w_i^b \varphi_a(\boldsymbol{r})\varphi_b(\boldsymbol{r})$$

where i/j and a/b are indices which represent the occupied and virtual molecular orbital (MO) respectively. w is the configuration coefficient of excitation. φ is the MO wavefunction. **r** is position vector. (Bold letters indicate vectors)

Sr exhibits the overlap of electron and hole density distributions:

$$S_r\ index = \int S_r(\boldsymbol{r})d\boldsymbol{r} = \int \sqrt{\rho^{hole}(\boldsymbol{r})\rho^{elec}(\boldsymbol{r})}d\boldsymbol{r}$$

D index means the centroid distance between hole and electron:

$$D\ index = \sqrt{|X_{elec} - X_{hole}|^2 + |Y_{elec} - Y_{hole}|^2 + |Z_{elec} - Z_{hole}|^2}$$

Here, X/Y/Z is coordinate of centroid of hole or electron. For example:

$$X_{elec} = \int x\rho^{elec}(\boldsymbol{r})d\boldsymbol{r}$$

and other coordinates can be shown in a similar manner.

The root-mean-square deviation (RMSD) of hole and electron reflect the extent of spatial distribution:

$$\sigma_{hole,\lambda} = \sqrt{\int (x - X_{hole})^2\rho^{hole}(\boldsymbol{r})d\boldsymbol{r}}$$

$$\sigma_{elec,\lambda} = \sqrt{\int (x - X_{elec})^2\rho^{elec}(\boldsymbol{r})d\boldsymbol{r}}$$

λ can be set as x, y, z.

H index implies the average degree of spatial extension:

$$H\ index = (|\boldsymbol{\sigma_{hole}}| + |\boldsymbol{\sigma_{elec}}|)/2$$

where $|\boldsymbol{\sigma_{hole}}|$ and $|\boldsymbol{\sigma_{elec}}|$ are magnitude of overall RMSD of hole and electron.

t index shows the separation degree of hole and electron in CT direction:

$$t\ index = D\ index - H_{CT}$$

Note that H_{CT} is expressed as:

$$H_{CT} = |\boldsymbol{H} \cdot \boldsymbol{u_{CT}}|$$

$$H_{\lambda} = (\sigma_{hole,\lambda} + \sigma_{elec,\lambda})/2$$

and $\boldsymbol{u_{CT}}$ is the unit vector in CT direction.

Table S10 Hole-electron analysis on the cations at the $S_0 \rightarrow S_1$ transition in the toluene. We performed the calculation using the optimized structures of the cations in the ground state.

$S_0 \rightarrow S_1$	S_r	D index (Å)	H index (Å)	t index (Å)
1	0.5755	4.246	3.355	1.306
2	0.6197	3.971	3.701	0.742
3	0.5883	4.632	3.836	1.320
4	0.5304	4.963	3.584	1.869
5	0.6320	3.690	3.652	0.502
6	0.5844	4.316	3.659	1.152
7	0.6346	3.950	3.843	0.578

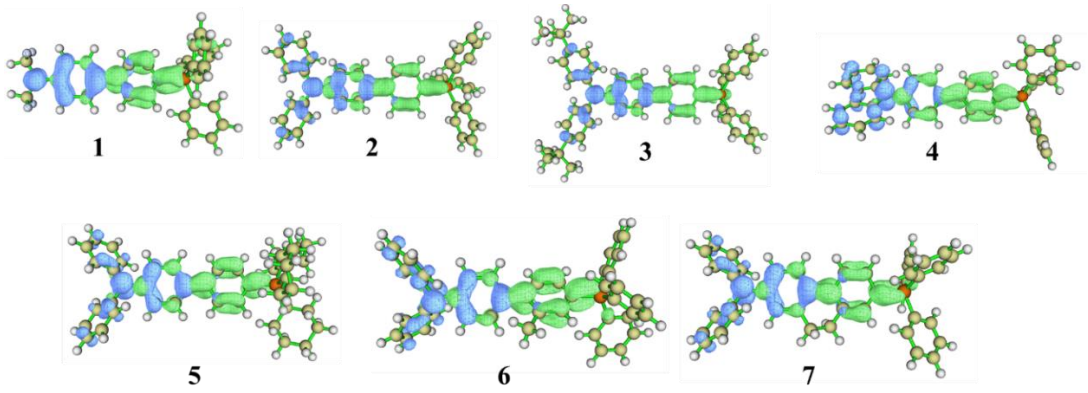

Fig. S14 Hole-electron distribution maps of the cations at $S_0 \rightarrow S_1$ transition in the toluene. Blue means the hole distribution and green means the electron distribution. All the surface of isovalue of map is set to 0.002.

Table S11 Hole-electron analysis on the cations at the S_0'→S_1' transition in the toluene. We performed the calculation using the optimized structures of the cations in the relaxed excited state.

S_0'→S_1'	S_r	D index (Å)	H index (Å)	t index (Å)
1	0.5349	4.144	3.395	1.150
2	0.5654	4.294	3.830	0.959
3	0.5179	5.133	3.935	1.793
4	0.5757	4.373	3.824	0.980
5	0.6028	3.741	3.707	0.512
6	0.5454	4.476	3.639	1.333
7	0.5731	4.236	3.694	1.004

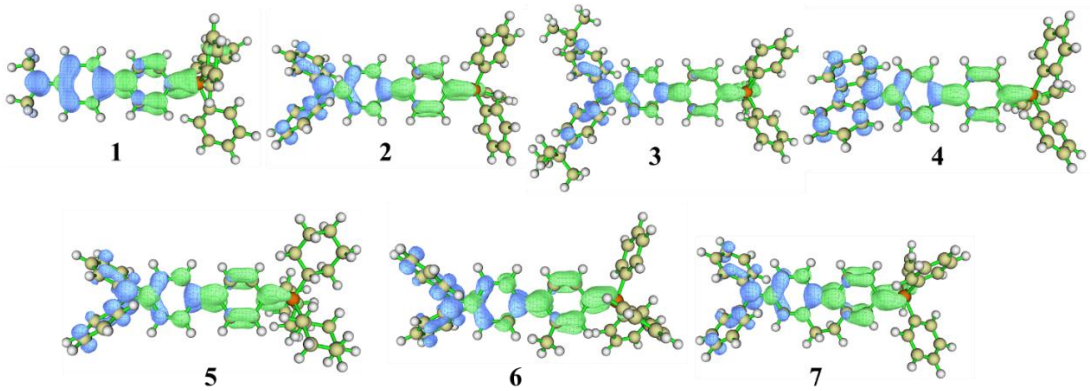

Fig. S15 Hole-electron distribution maps of the cations at the S_0'→S_1' transition in the toluene. Blue means the hole distribution and green means the electron distribution. All the surface of isovalue of map is set to 0.002.

The atomic charges were determined by restrained electrostatic potential (RESP)[22,23] calculation in Multiwfn. We also used Visual molecular dynamics (VMD) to visualize the electrostatic potential maps of the cations based on the RESP calculations. By this method, we could distinguish the strength of donor or acceptor obviously. The translocation rate of anion is influenced by the Coulomb interaction between the anion and the atoms belonging to the donor/acceptor. Our proposed models (Fig. S18-S20) maintain a distance of 6 Å between the negative charge center (**[OTF]**$^-$ anion) and the phosphorus (acceptor) or nitrogen (donor) atom. The resultant force acting on the negative charge center (Table S12) can be used as an indicator to determine the positive charge localization of cation backbone.

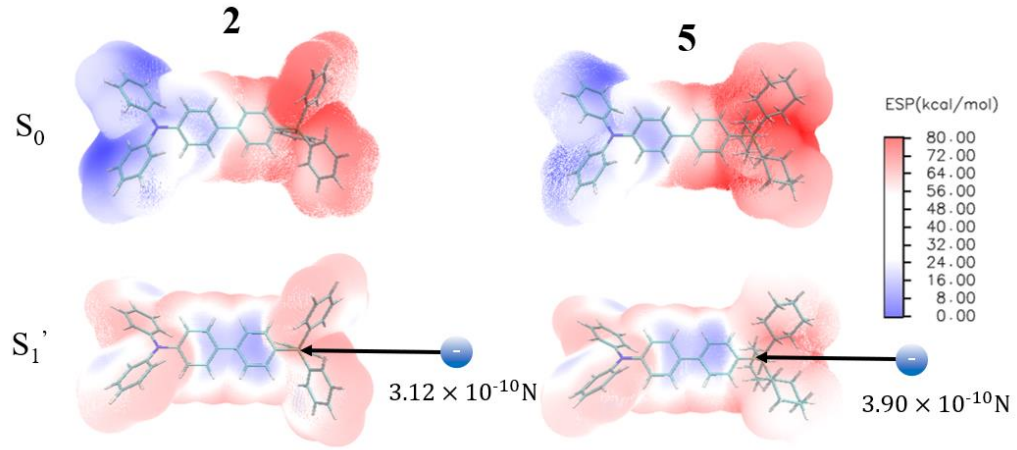

Fig. S16 Electrostatic potential maps of the cations in Group B calculated by the restrained electrostatic potential (RESP) method. We also exhibit the coulombic interaction between the anion and the atoms of acceptor here. (see model in Fig. S19)

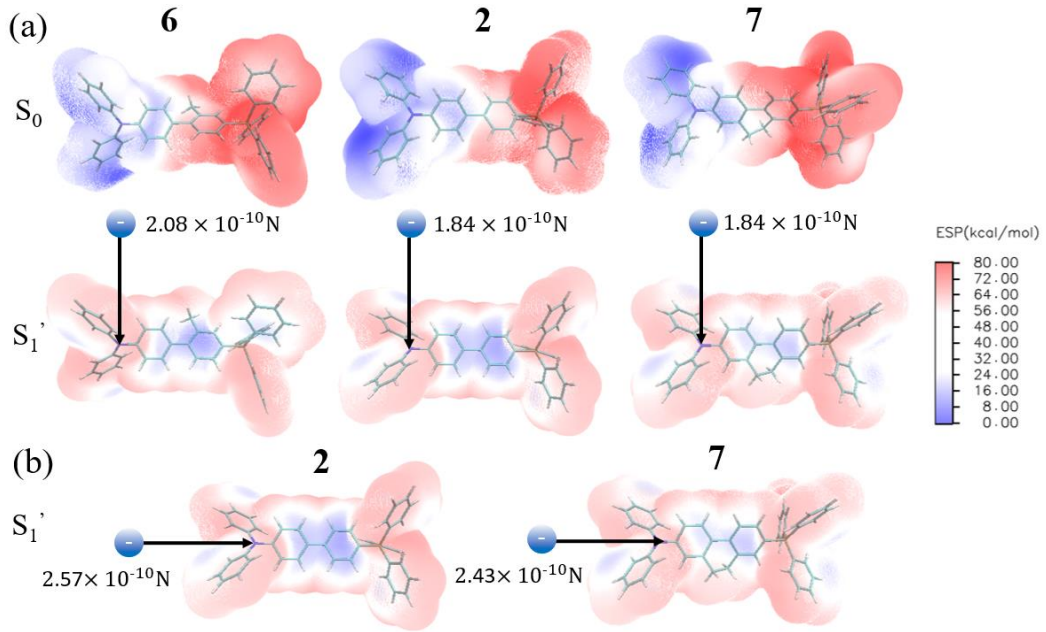

Fig. S17 (a) Electrostatic potential maps of the cations in Group C calculated by the restrained electrostatic potential (RESP) method. We also exhibit the coulombic interaction between the anion and the atoms of acceptor in (a) and (b). (see models in Figure S20(a) and (b))

Table S12 The net electrostatic interaction acting on the negatively charged center based on models in Figure S18-S20.

		Coulomb force (10^{-10}N)
(a)	**1**	2.81
	2	1.84
	3	1.76
	4	1.48
	6	2.08
	7	1.84
(b)	**2**	3.12
	5	3.90
(c)	**2**	2.57
	7	2.43

(a) is calculated using a model where the negative charge center is perpendicular to the donor plane, and the distance between the negative charge center and the nitrogen (blue) atom is fixed at 6 Å, e.g., 1 in the Fig. S18. (b) is calculated using a model where the distance between the negative charge center and the phosphorus atom is kept at 6 Å along the z-axis (CT direction), e.g., 5 in the Fig. S19. (c) is calculated using a model where the distance between the negative charge center and the nitrogen atom is kept at 6 Å along the z-axis (CT direction), e.g., 2 in Fig. S20(b).

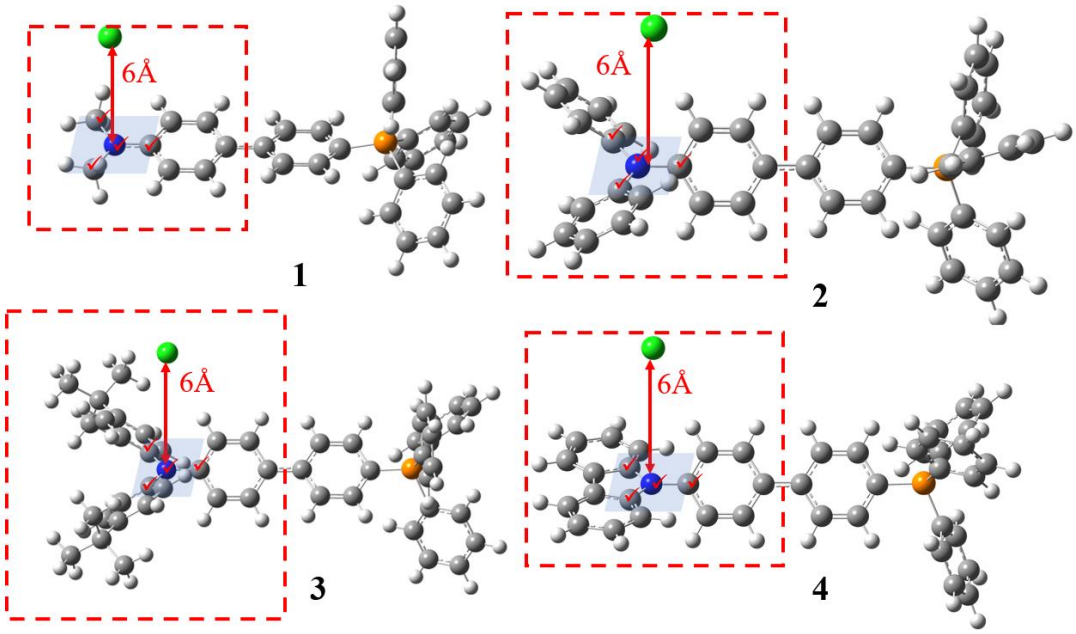

Fig. S18 The models of Group A cations for calculating Coulomb interaction. The negative charge center (green) is located normal to the donor plane (labeled with red tick), with the distance between the negative charge center and the nitrogen (blue) atom is fixed at 6 Å. The net Coulomb interaction acting on the negative charge center is calculated with respect to the other atoms within the red frame (the same as Fig. S19 and S20).

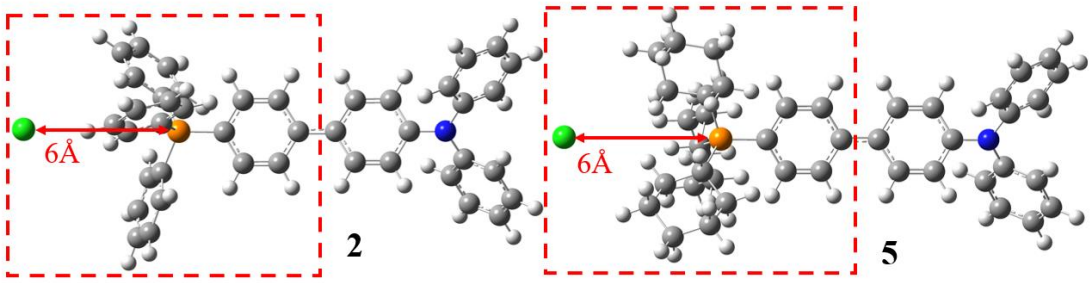

Fig. S19 The models of Group B cations for calculating Coulomb interaction. The negative charge center (green) is placed along the z-axis (CT direction), with the distance between the negative charge center and the phosphorus (orange) atom is fixed at 6 Å.

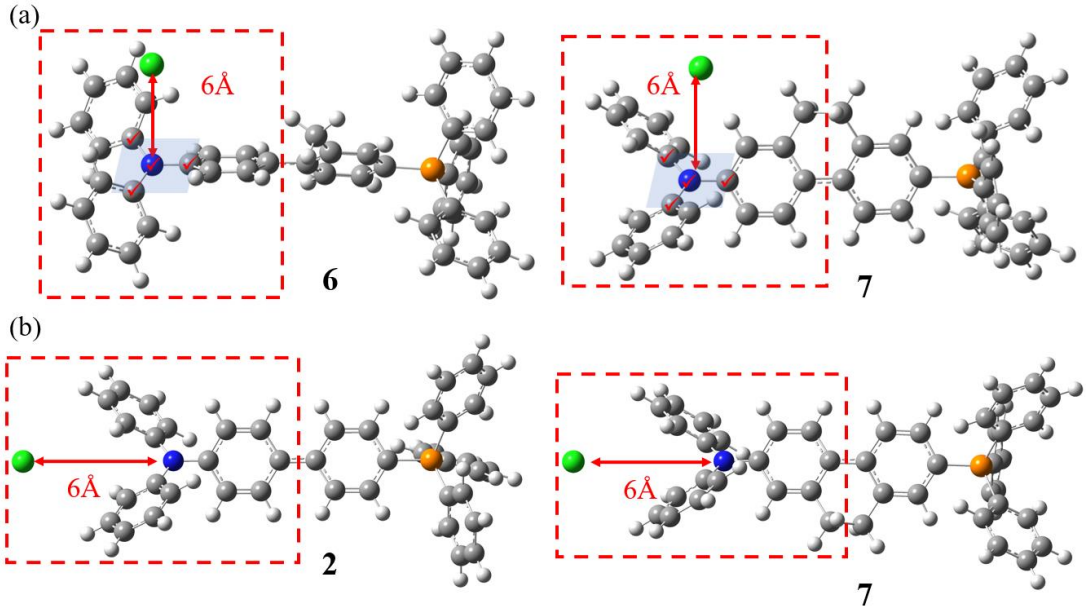

Fig. S20 (a) The models of Group C cations for calculating Coulomb interaction. The negative charge center (green) is located normal to the donor plane (labeled with red tick), with the distance between the negative charge center and the nitrogen (blue) atom is fixed at 6 Å. (b) To eliminate the influence of the positive charge on the biphenyl bridge, we place the negative charge center along the z-axis (CT direction), maintaining a 6 Å distance between the negative charge center and the nitrogen atom. This ensures that the biphenyl bridge is far from the negatively charged center compared to the former and the results show that **2** has stronger Coulomb interaction acting on the negative charge center.

Table S13 The dipole moment of cation backbone in the ground state (S_0) and excited state (S_1') after relaxation. Note: The calculation does not include the counter anion. The discrepancy between the experimental and computational results may be due to the influence of anion. (unit: debye)

Dipole moment in S_0		Dipole moment in S_1'	
1	5.3287	1'	11.7234
2	17.1897	2'	0.9481
3	23.6586	3'	2.6289
4	20.8944	4'	0.2320
5	15.4845	5'	1.6648
6	17.3755	6'	1.7431
7	16.7723	7'	1.4013

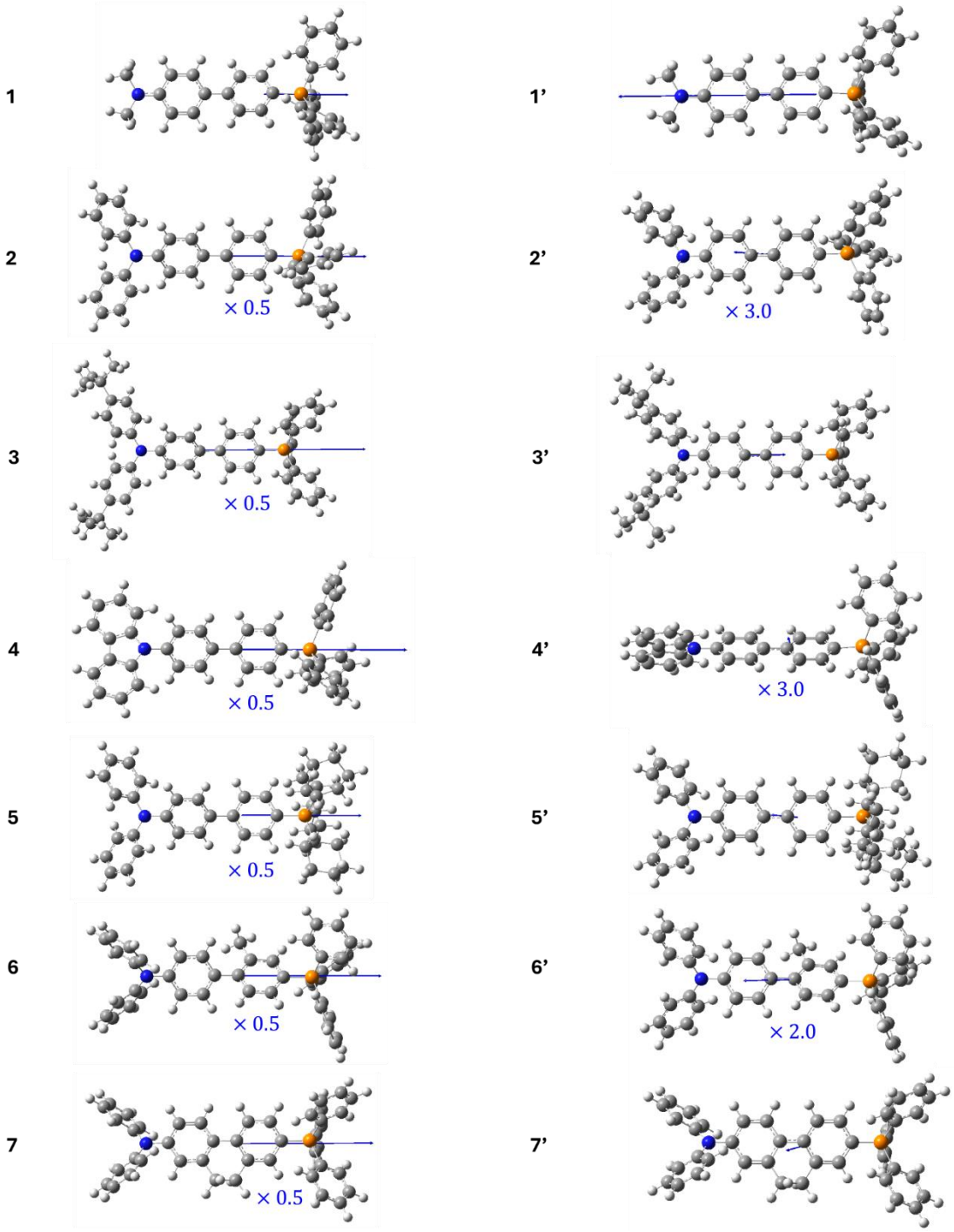

Fig. S21 The left column displays the permanent dipole moments of the entitled compounds (**1**-**7**) optimized in the ground state (S_1'). The right column presents the permanent dipole moments of the same structures optimized in the excited state (S_1) which are mark as 1'-7'.

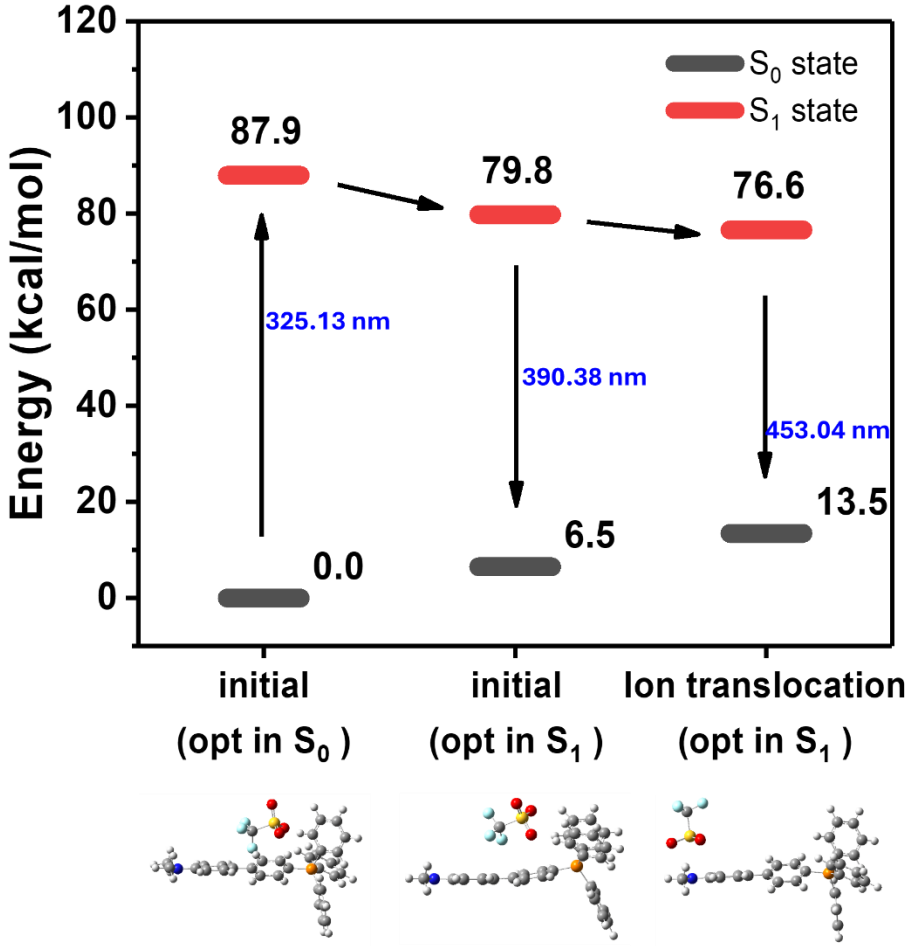

Fig. S22 In the S1 state, the anion translocation process of compound **1** effectively reduces the energy level, resulting in a red-shift in the emission (from 390.38 nm to 453.04 nm).

5.NMR Appendix

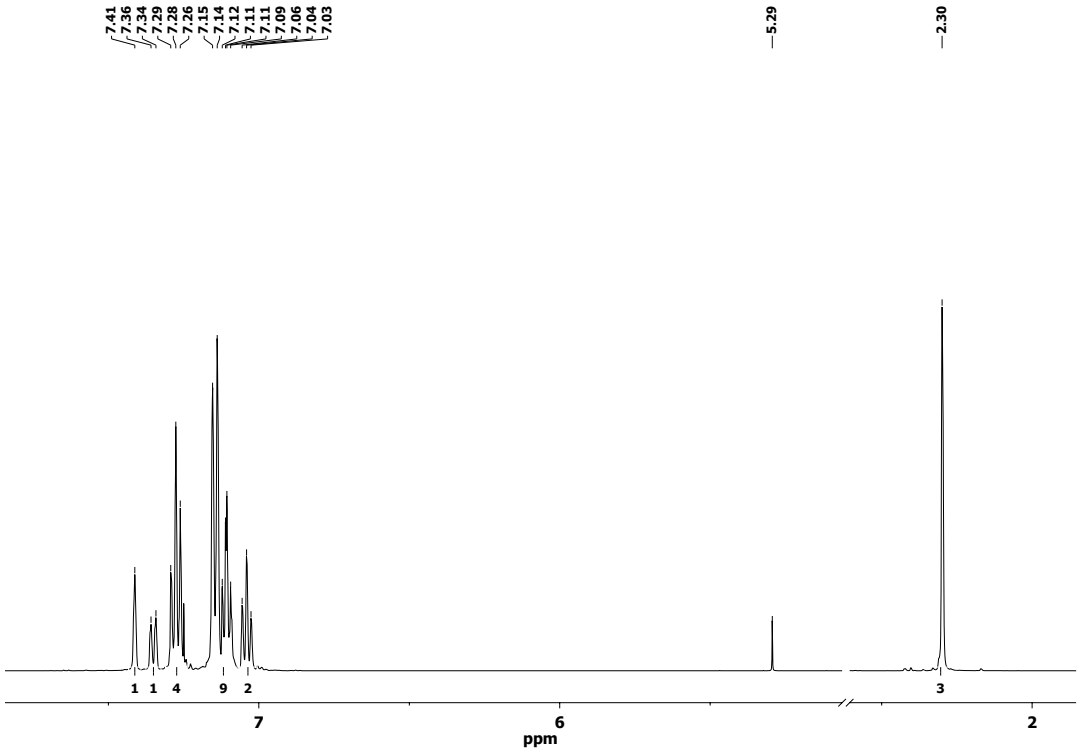

Fig. S23 ^{1}H NMR spectrum of **a1**, measured in $CDCl_3$ at 298K.

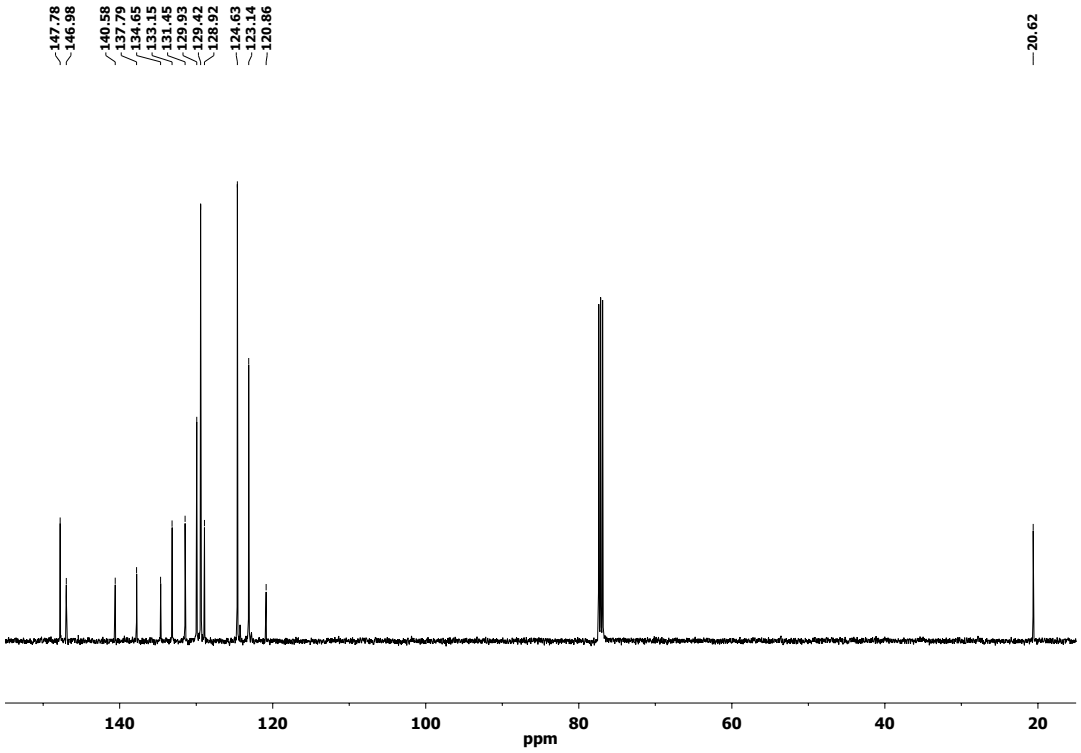

Fig. S24 ^{13}C NMR spectrum of **a1**, measured in $CDCl_3$ at 298K.

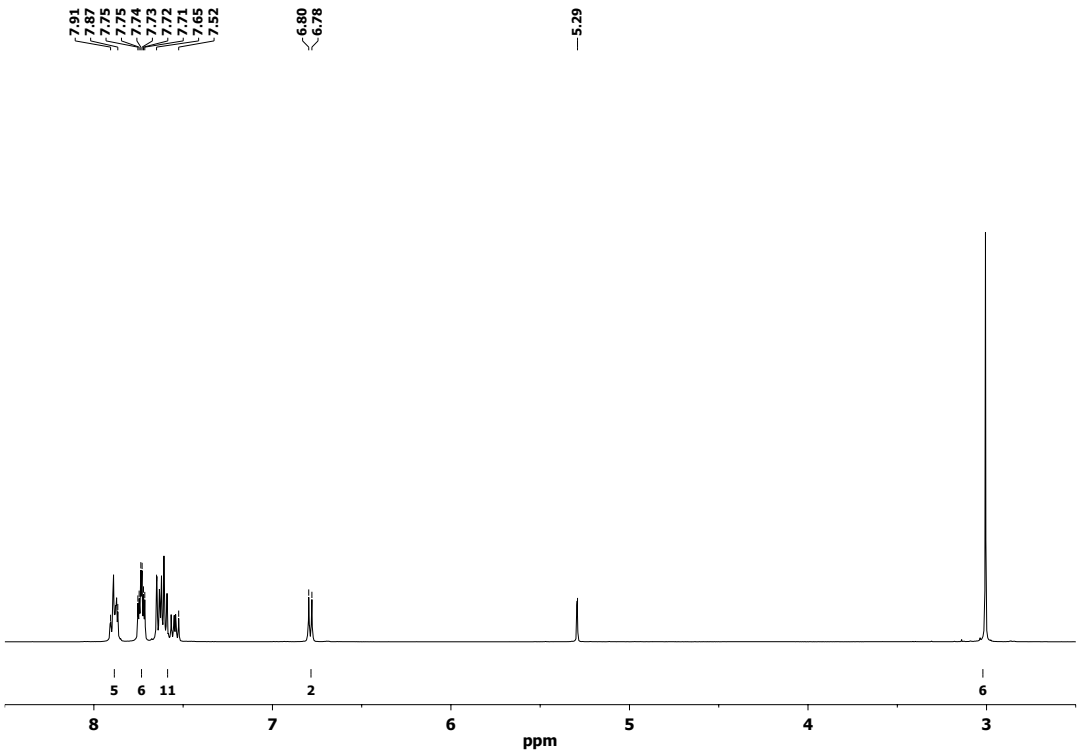

Fig. S25 ^{1}H NMR spectrum of **1[OTf]**, measured in CD_2Cl_2 at 298K.

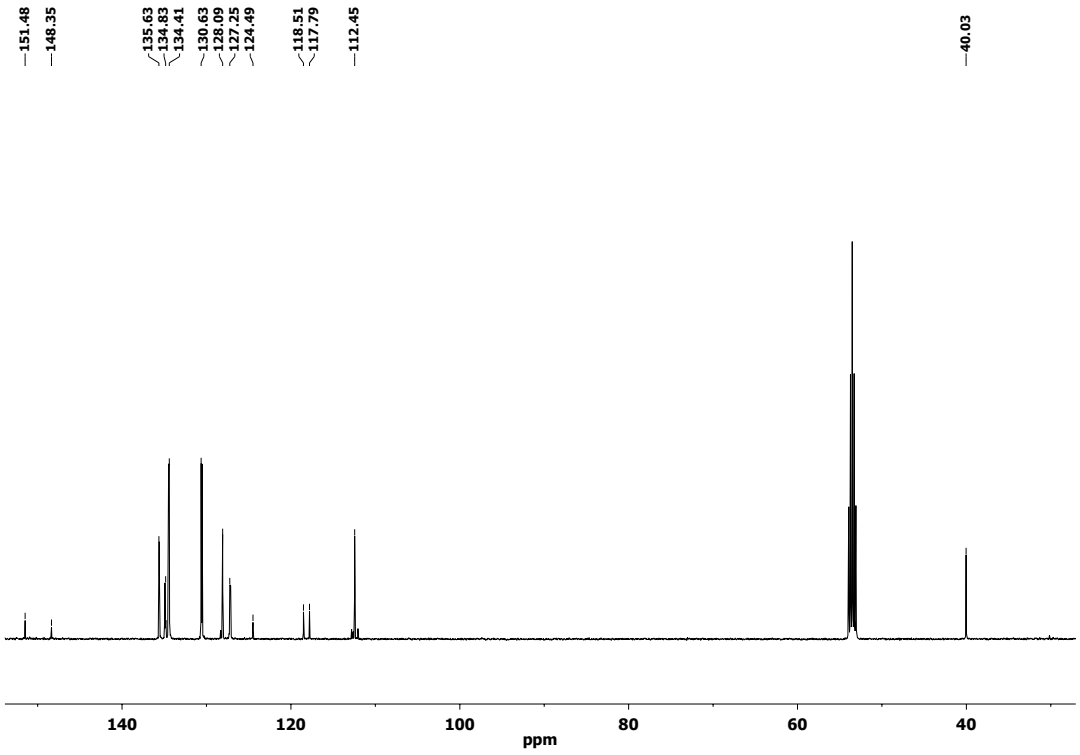

Fig. S26 ^{13}C NMR spectrum of **1[OTf]**, measured in CD_2Cl_2 at 298K.

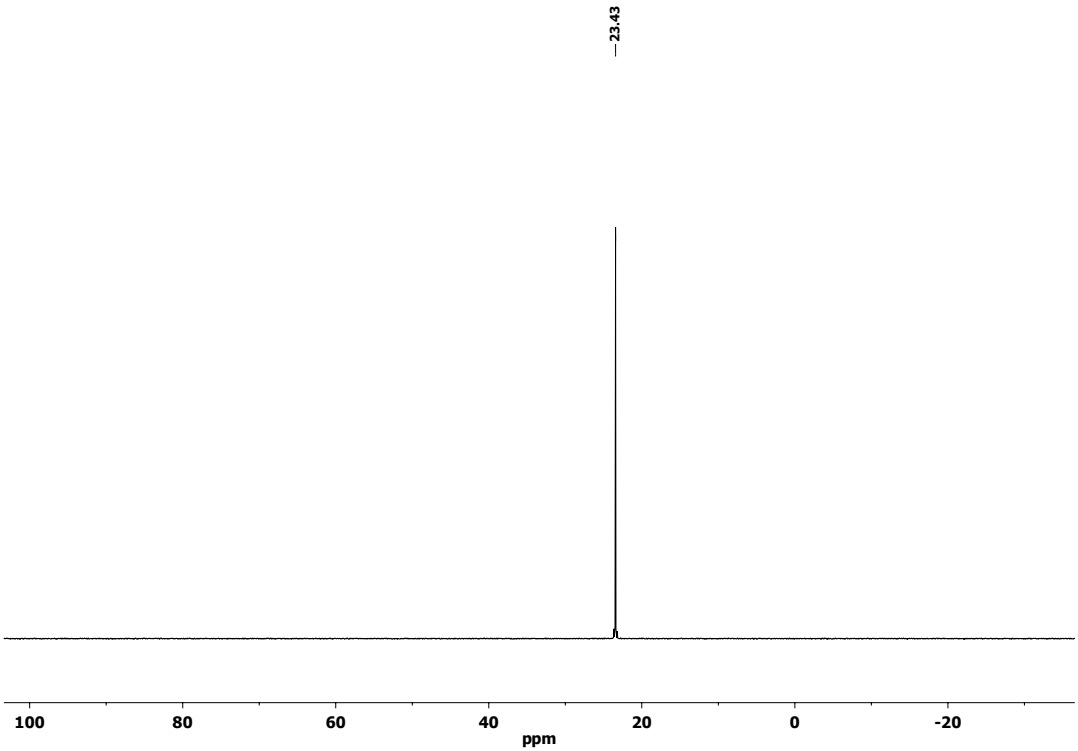

Fig. S27 ^{31}P NMR spectrum of **1[OTf]**, measured in CD_2Cl_2 at 298K.

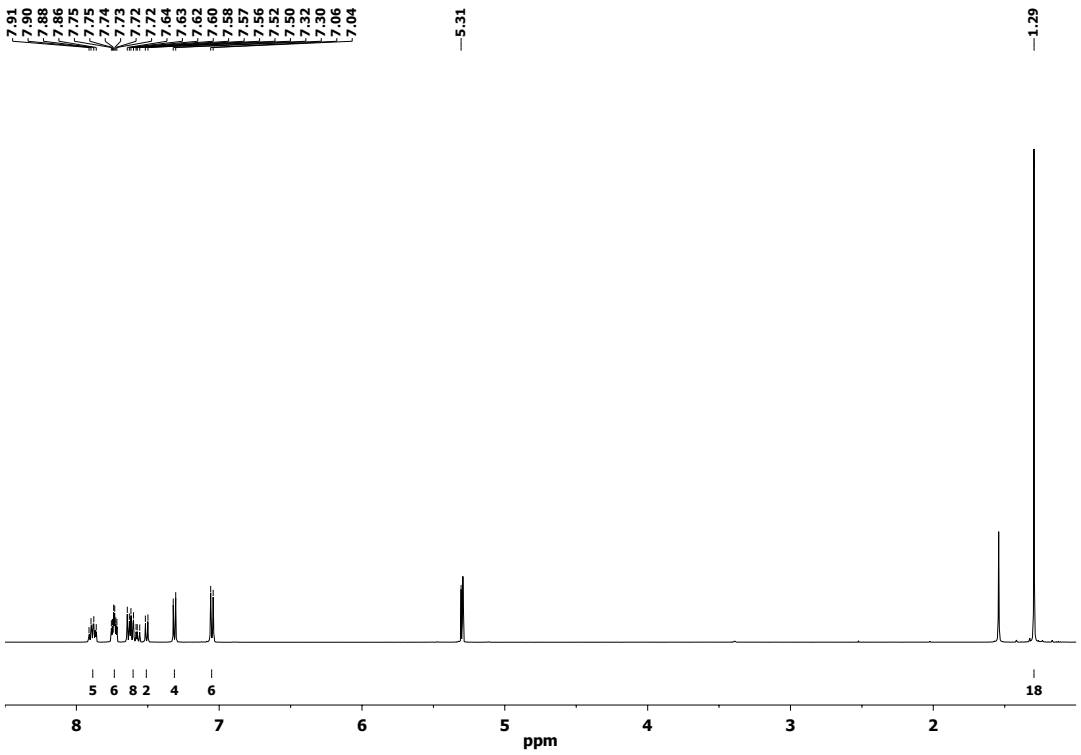

Fig. S28 ^{1}H NMR spectrum of **3[OTf]**, measured in CD_2Cl_2 at 298K.

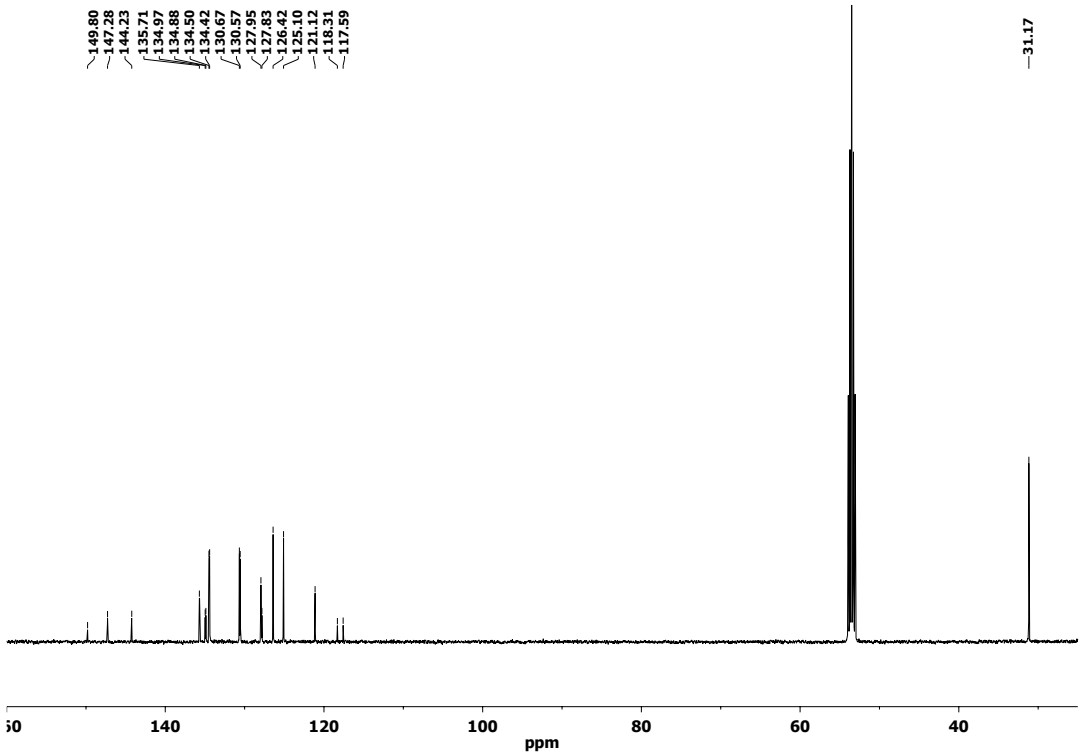

Fig. S29 ^{13}C NMR spectrum of **3[OTf]**, measured in CD_2Cl_2 at 298K.

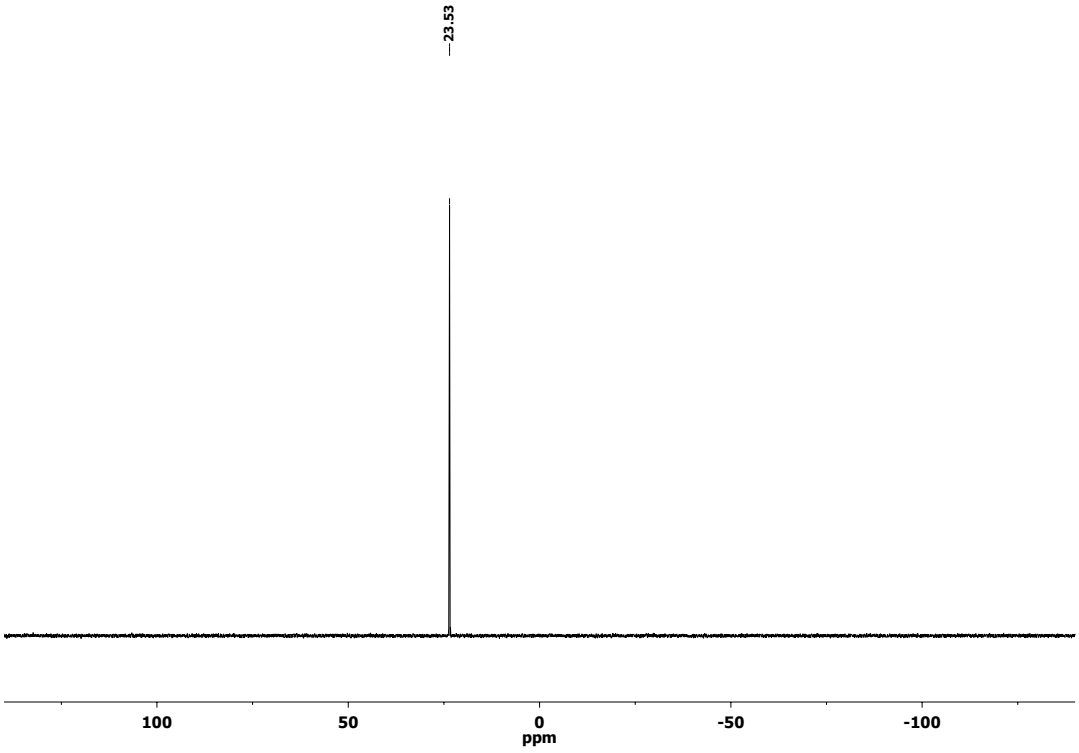

Fig. S30 ^{31}P NMR spectrum of **3[OTf]**, measured in CD_2Cl_2 at 298K.

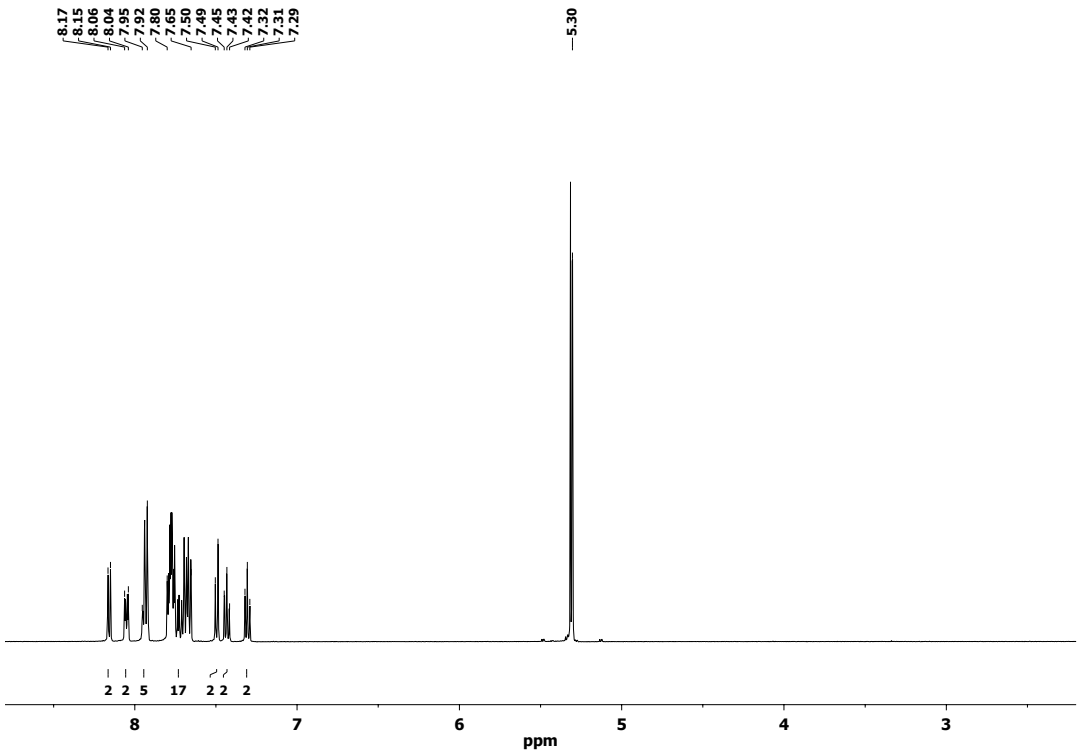

Fig. S31 ^{1}H NMR spectrum of **4[OTf]**, measured in CD_2Cl_2 at 298K.

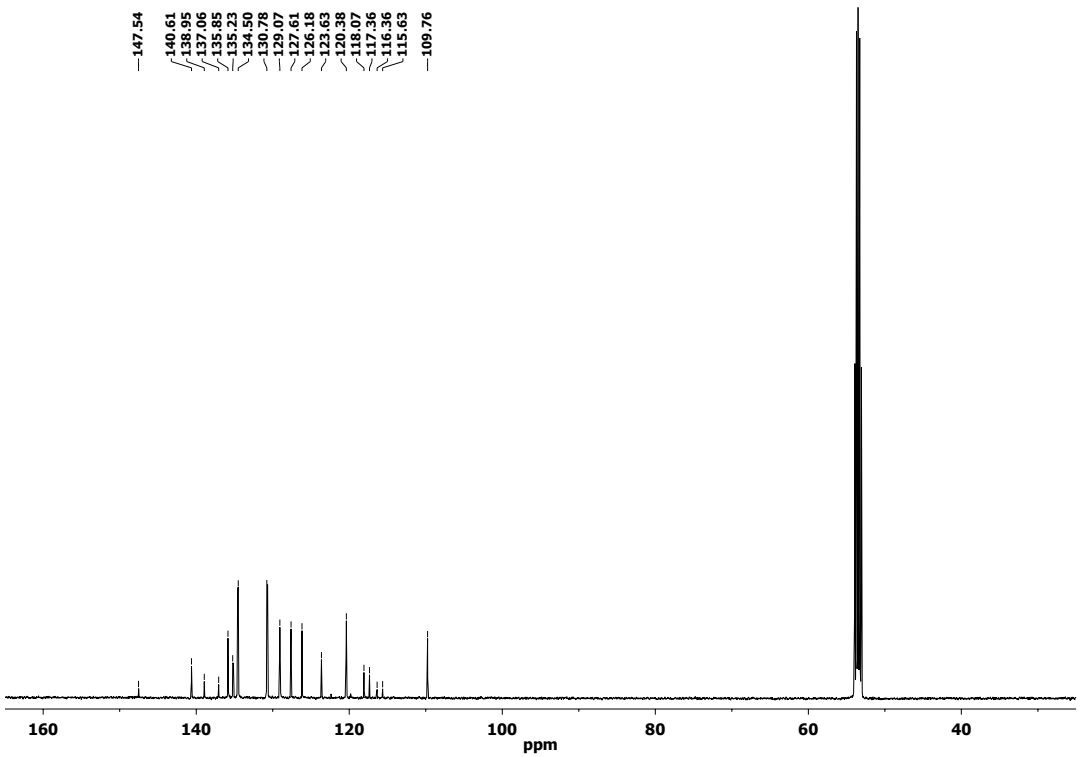

Fig. S32 ^{13}C NMR spectrum of **4[OTf]**, measured in CD_2Cl_2 at 298K.

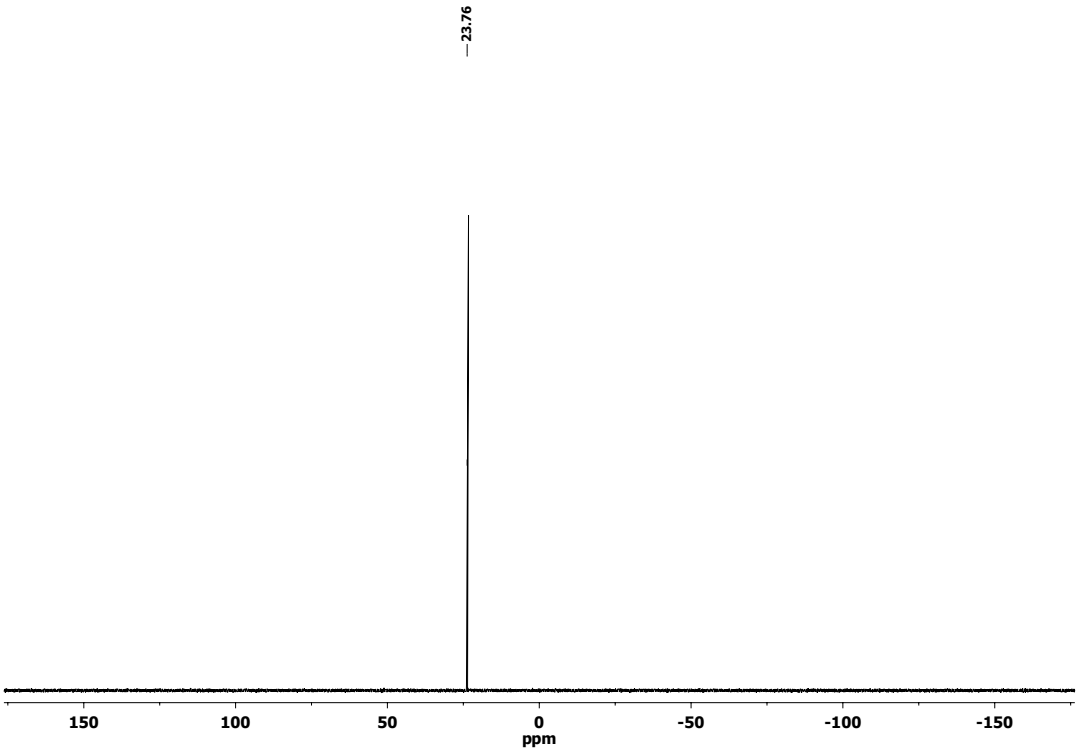

Fig. S33 ^{31}P NMR spectrum of **4[OTf]**, measured in CD_2Cl_2 at 298K.

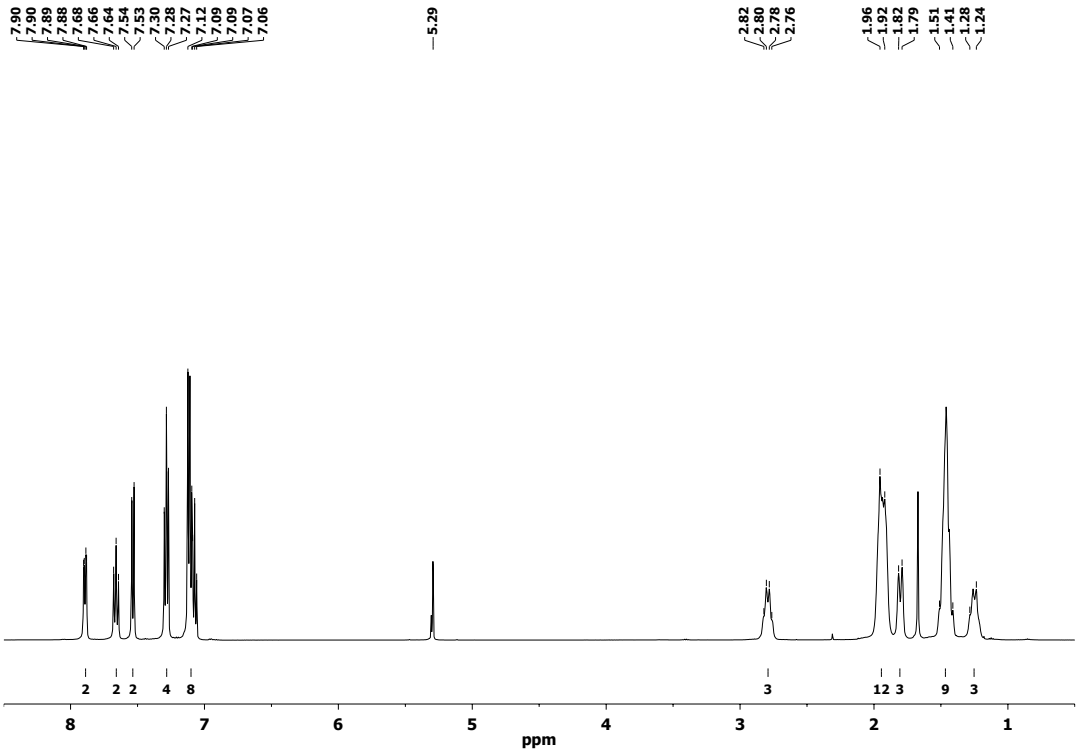

Fig. S34 ^{1}H NMR spectrum of **5[OTf]**, measured in CD_2Cl_2 at 298K.

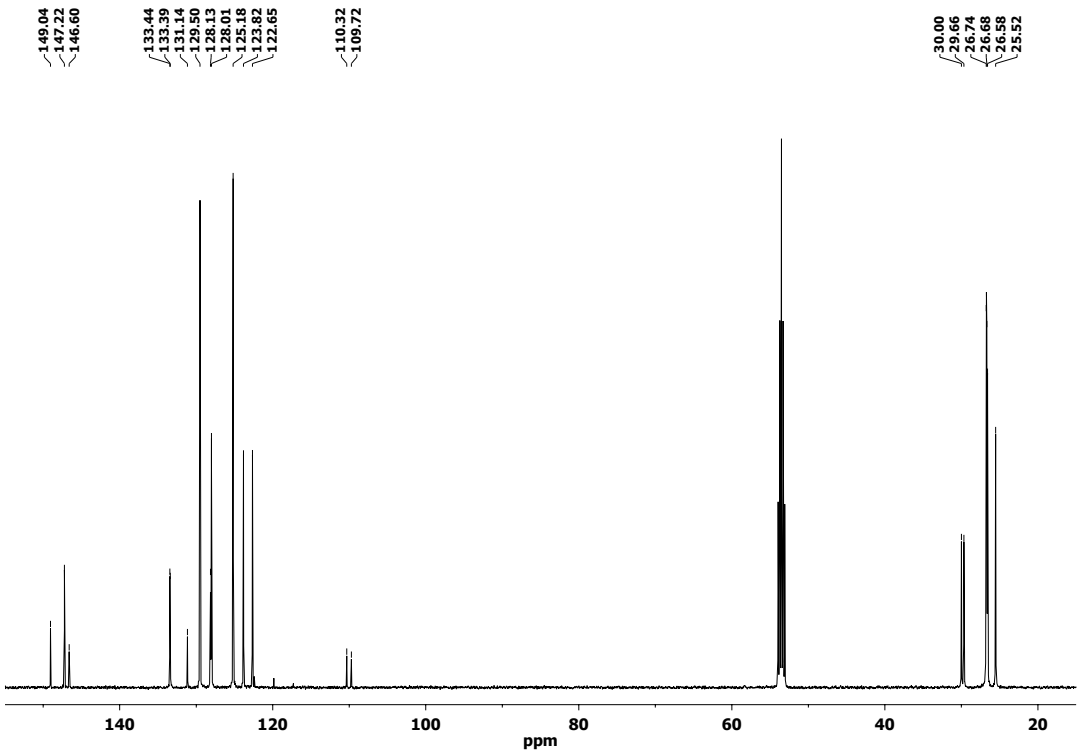

Fig. S35 ^{13}C NMR spectrum of **5[OTf]**, measured in CD_2Cl_2 at 298K.

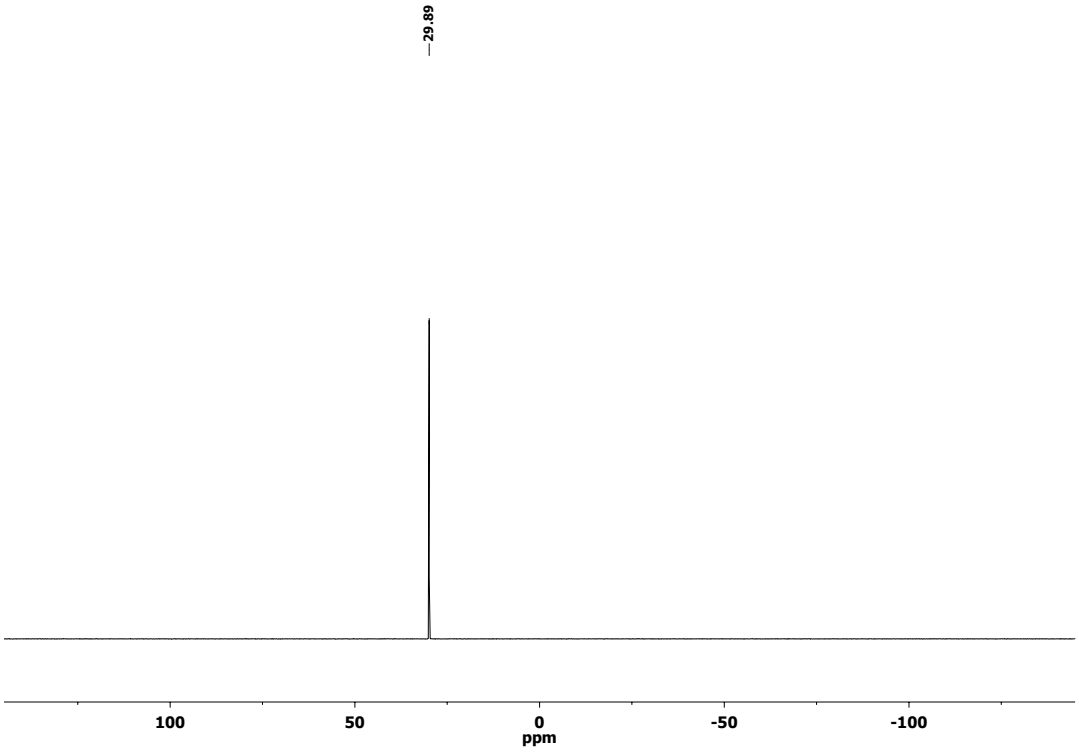

Fig. S36 ^{31}P NMR spectrum of **5[OTf]**, measured in CD_2Cl_2 at 298K.

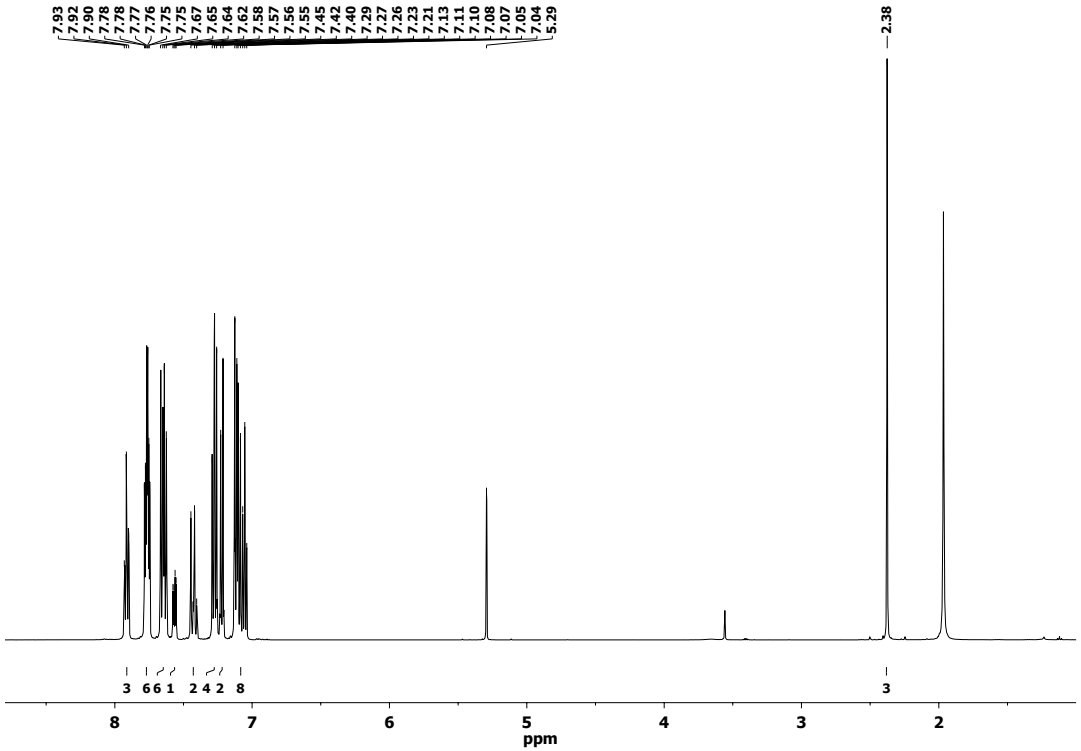

Fig. S37 ^{1}H NMR spectrum of **6[OTf]**, measured in CD_2Cl_2 at 298K.

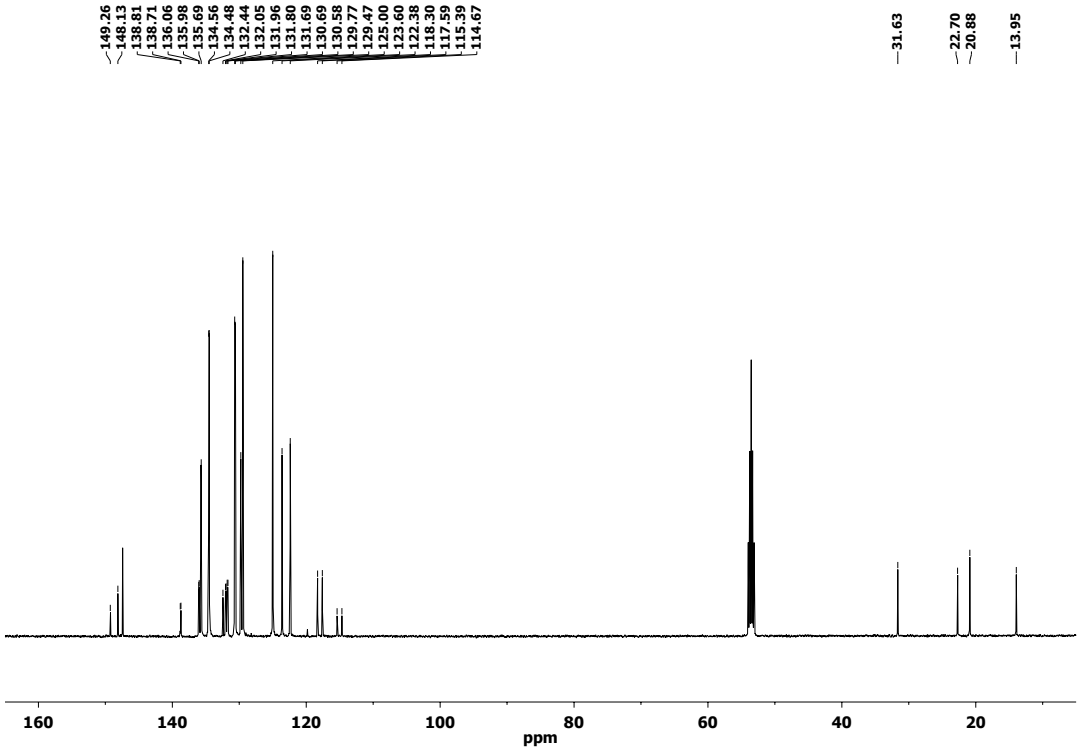

Fig. S38 ^{13}C NMR spectrum of **6[OTf]**, measured in CD_2Cl_2 at 298K.

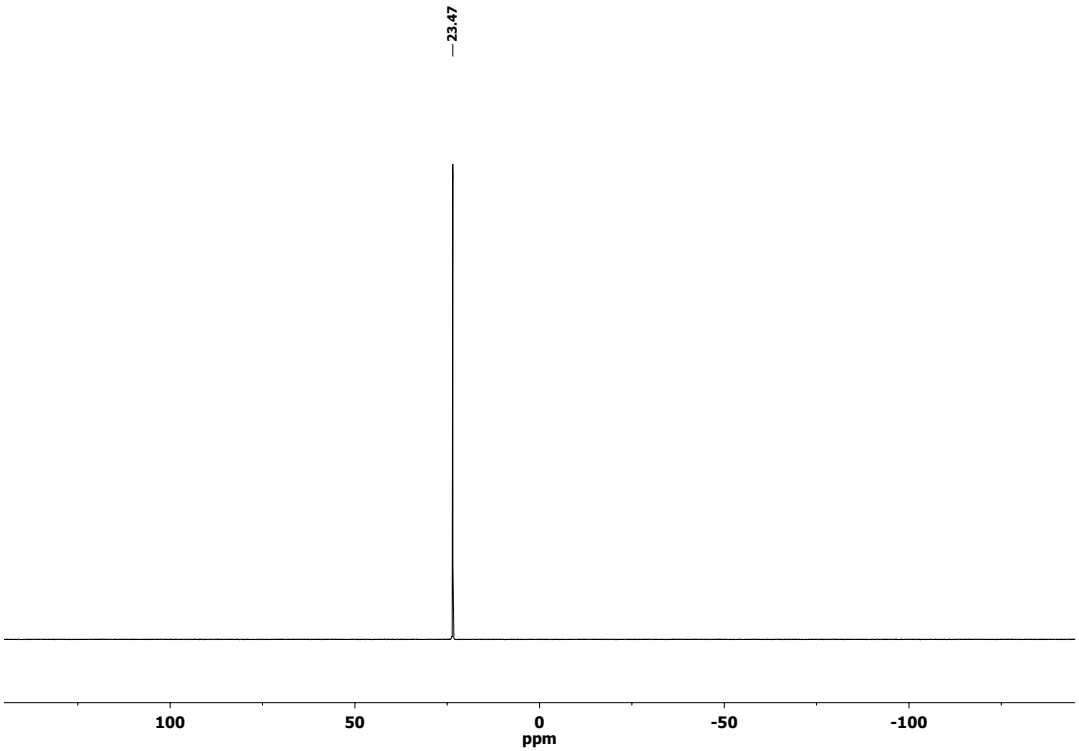

Fig. S39 ^{31}P NMR spectrum of **6[OTf]**, measured in CD_2Cl_2 at 298K.

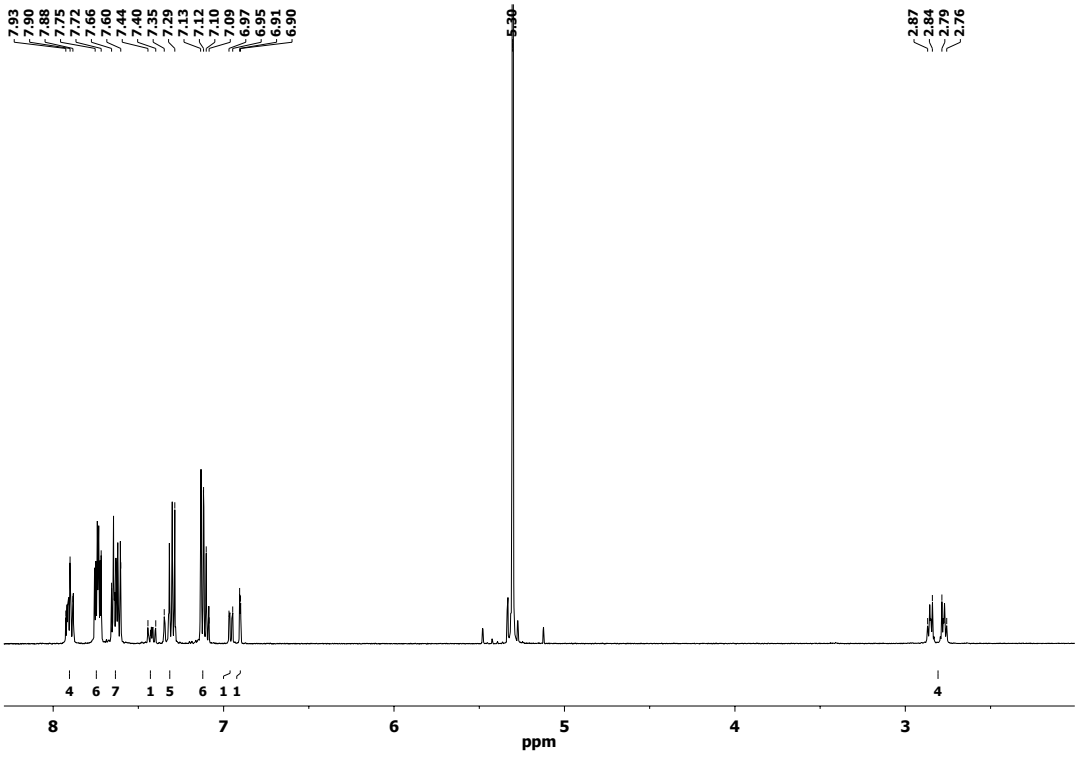

Fig. S40 ^{1}H NMR spectrum of **7[OTf]**, measured in CD_2Cl_2 at 298K.

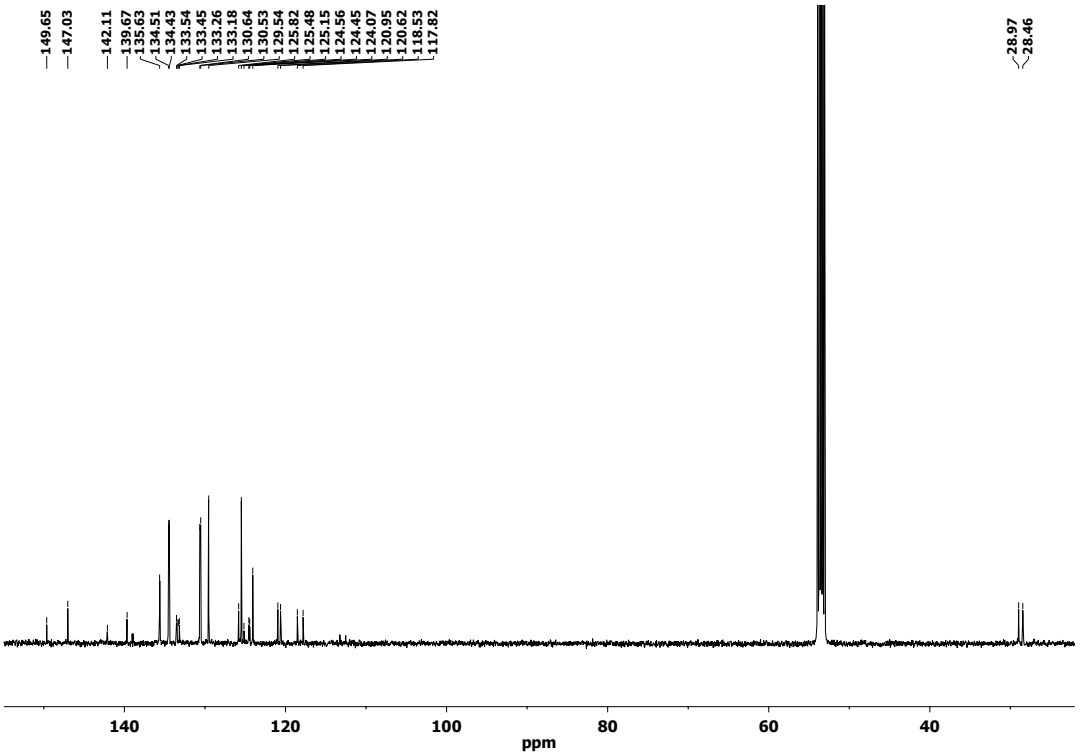

Fig. S41 ^{13}C NMR spectrum of **7[OTf]**, measured in CD_2Cl_2 at 298K.

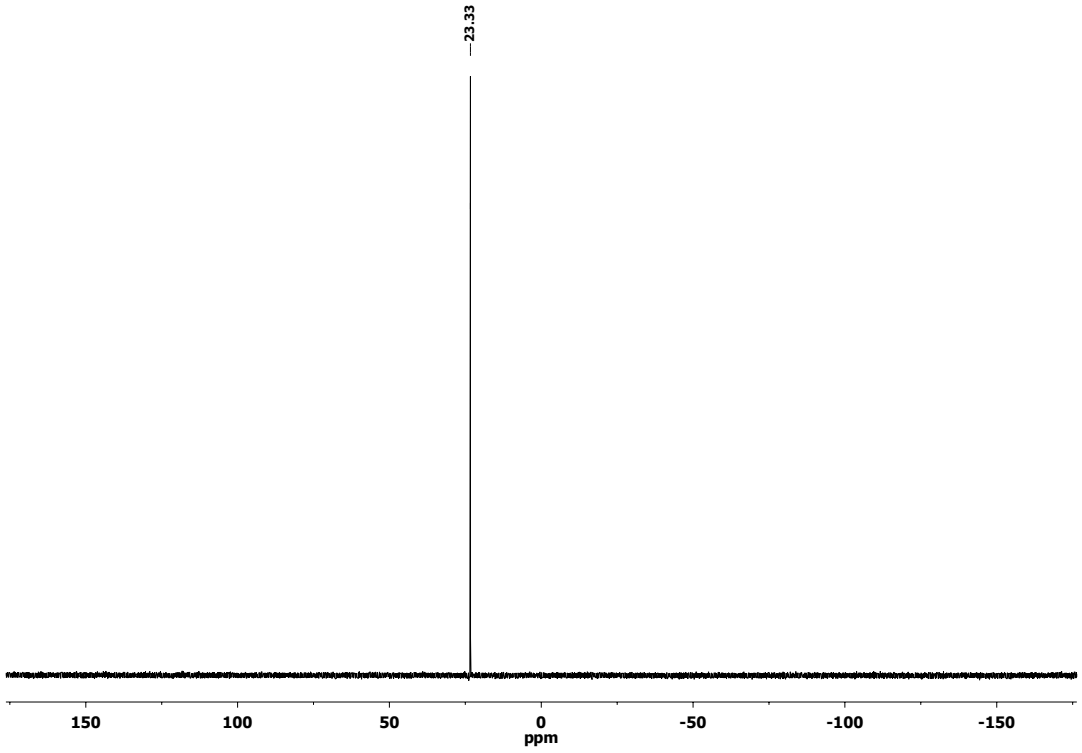

Fig. S42 ^{31}P NMR spectrum of **7[OTf]**, measured in CD_2Cl_2 at 298K.

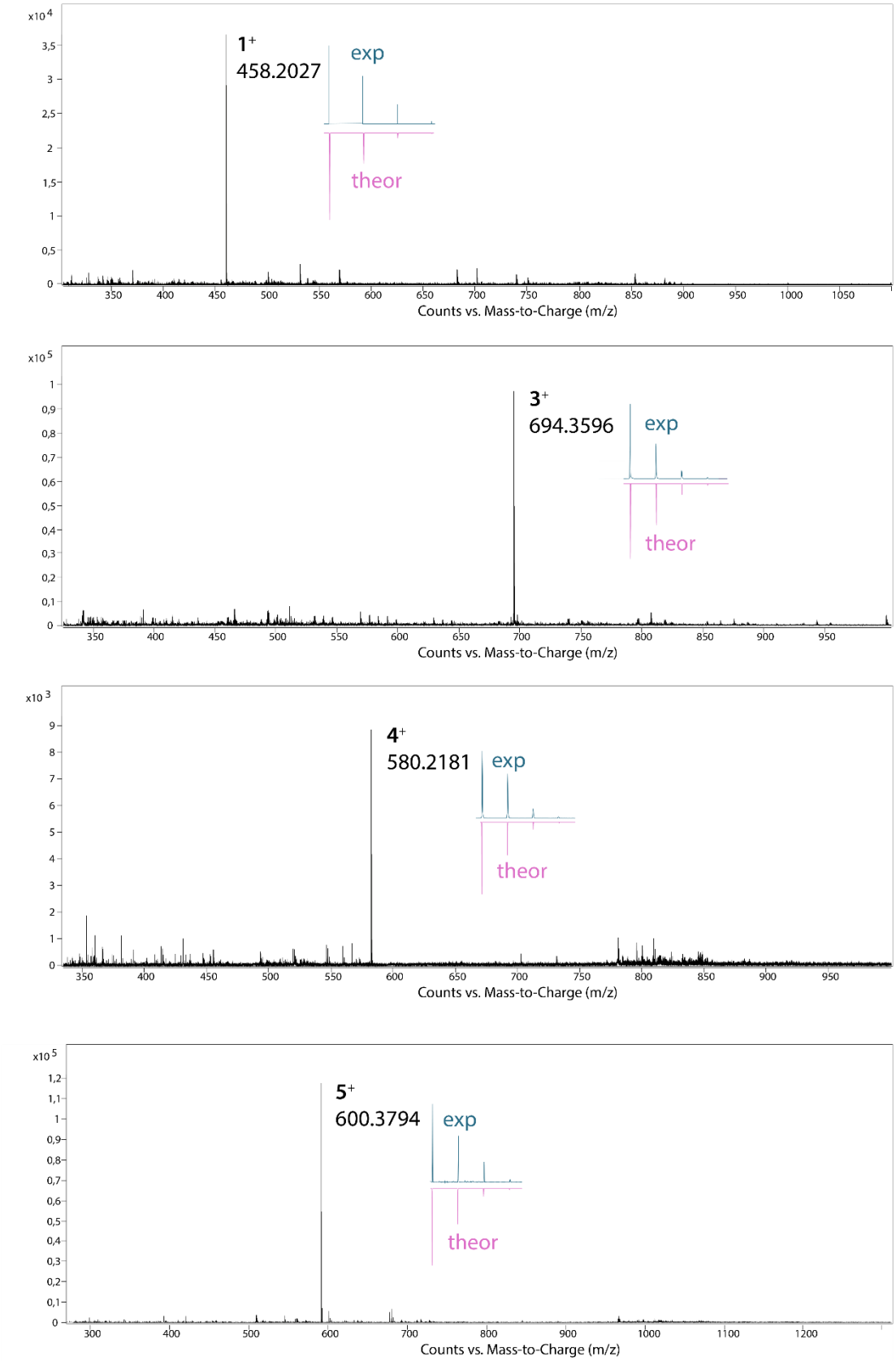

Fig. S43 ESI⁺ mass spectra of **1,3–5[OTf]** salts, insert shows experimental (green) and theoretical (pink) isotopic distribution of the signal.

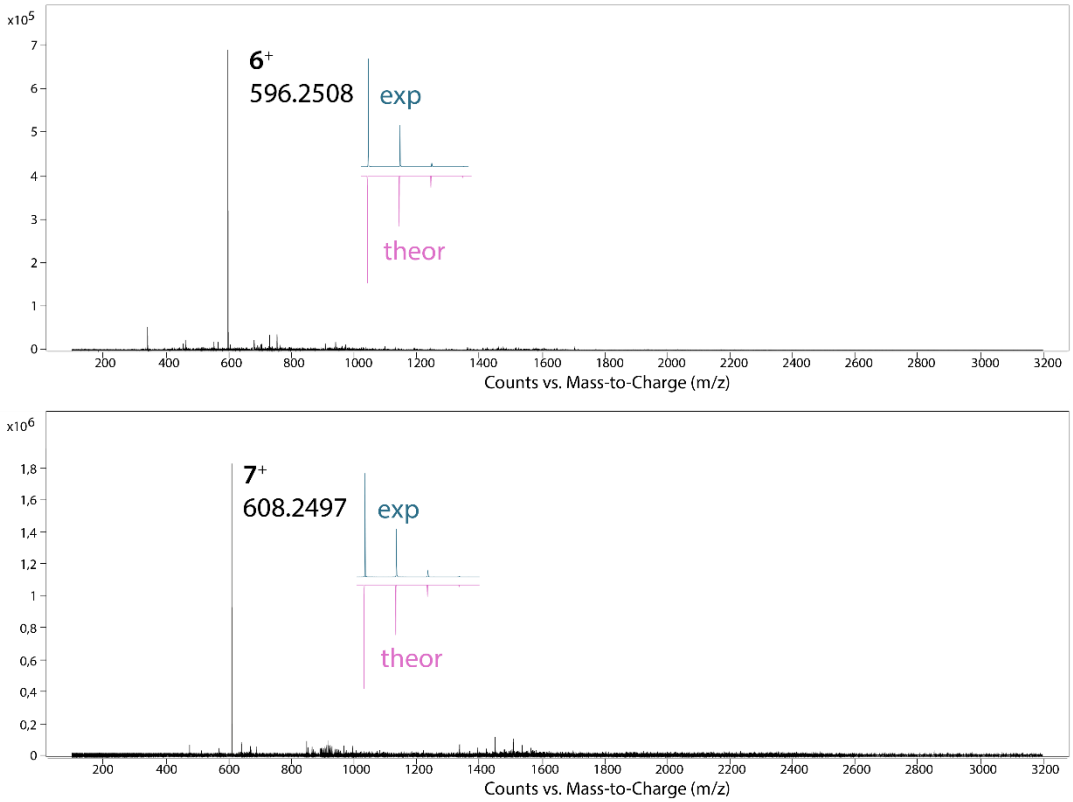

Fig. S44 ESI$^+$ mass spectra of **6–7[OTf]** salts, insert shows experimental (green) and theoretical (pink) isotopic distribution of the signal.

6.Reference

(1) R. Y.-Y. Lin, Y.-S. Yen, Y.-T. Cheng, C.-P. Lee, Y.-C. Hsu, H.-H. Chou, C.-Y. Hsu, Y.-C. Chen, J. T. Lin and K.-C. Ho, Dihydrophenanthrene-based metal-free dyes for highly efficient cosensitized solar cells, *Organic letters*, 2012, **14**, 3612-3615.

(2) X. Yang, Y. Zhao, X. Zhang, R. Li, J. Dang, Y. Li, G. Zhou, Z. Wu, D. Ma and W.-Y. Wong, Thiazole-based metallophosphors of iridium with balanced carrier injection/transporting features and their two-colour WOLEDs fabricated by both vacuum deposition and solution processing-vacuum deposition hybrid strategy, *Journal of Materials Chemistry*, 2012, **22**, 7136-7148

(3) T.-C. Lin, Z.-Y. Liu, S.-H. Liu, I. O. Koshevoy and P.-T. Chou, Counterion migration driven by light-induced intramolecular charge transfer, *JACS Au*, 2021, **1**, 282-293.

(4) Z. H. Li, M. S. Wong, Y. Tao and M. D'Iorio, Synthesis and functional properties of strongly luminescent diphenylamino end-capped oligophenylenes, *The Journal of Organic Chemistry*, 2004, **69**, 921-927.

(5) D. Oesch and N. W. Luedtke, Fluorescent chemosensors of carbohydrate triols exhibiting TICT emissions, *Chemical Communications*, 2015, **51**, 12641-12644.

(6) A. Belyaev, Y. H. Cheng, Z. Y. Liu, A. J. Karttunen, P. T. Chou and I. O. Koshevoy, A Facile Molecular Machine: Optically Triggered Counterion Migration by Charge Transfer of Linear Donor-π-Acceptor Phosphonium Fluorophores, *Angewandte Chemie International Edition*, 2019, **58**, 13456-13465.

(7) G. M. Sheldrick, Crystal structure refinement with SHELXL, *Acta Crystallographica Section C: Structural Chemistry*, 2015, **71**, 3-8.

(8) G. M. Sheldrick, SHELXT–Integrated space-group and crystal-structure determination, *Acta Crystallographica Section A: Foundations and Advances*, 2015, **71**, 3-8.

(9) A. N. Fletcher and D. E. Bliss, Laser dye stability. Part 5: Effect of chemical substituents of bicyclic dyes upon photodegradation parameters, *Applied physics*, 1978, **16**, 289-295.

(10) C. Würth, M. Grabolle, J. Pauli, M. Spieles and U. Resch-Genger, Comparison of methods and achievable uncertainties for the relative and absolute measurement of photoluminescence quantum yields, *Analytical chemistry*, 2011, **83**, 3431-3439.

(11) A. Koti, M. Krishna and N. Periasamy, Time-resolved area-normalized emission spectroscopy (TRANES): a novel method for confirming emission from two excited states, *The Journal of Physical Chemistry A*, 2001, **105**, 1767-1771.

(12) A. Barlow, J. Lamb and A. Matheson, Viscous behaviour of supercooled liquids, *Proceedings of the Royal Society of London. Series A. Mathematical and Physical Sciences*, 1966, **292**, 322-342.

(13) K. R. Harris, Temperature and density dependence of the viscosity of toluene, *Journal of Chemical & Engineering Data*, 2000, **45**, 893-897.

(14) A. Messaâdi, N. Dhouibi, H. Hamda, F. B. M. Belgacem, Y. H. Adbelkader, N. Ouerfelli and A. H. Hamzaoui, A new equation relating the viscosity Arrhenius temperature and the activation energy for some Newtonian classical solvents, *Journal of Chemistry*, 2015, **2015**, 163262.

(15) L. Snoussi, S. Babu, J. V. Herráez, S. Akhtar, A. Al-Arfaj and N. Ouerfelli, Thermodynamic parameters modeling of viscous flow activation in ethylene glycol-water fluid systems, *Iranian Journal of Chemistry and*

Chemical Engineering, 2020, **39**, 287-301.

(16) M. J. Frisch, G. W. Trucks, H. B. Schlegel, G. E. Scuseria, M. A. Robb, J. R. Cheeseman, G. Scalmani, V. Barone, G. A. Petersson, H. Nakatsuji, X. Li, M. Caricato, A. V. Marenich, J. Bloino, B. G. Janesko, R. Gomperts, B. Mennucci, H. P. Hratchian, J. V. Ortiz, A. F. Izmaylov, J. L. Sonnenberg, Williams, F. Ding, F. Lipparini, F. Egidi, J. Goings, B. Peng, A. Petrone, T. Henderson, D. Ranasinghe, V. G. Zakrzewski, J. Gao, N. Rega, G. Zheng, W. Liang, M. Hada, M. Ehara, K. Toyota, R. Fukuda, J. Hasegawa, M. Ishida, T. Nakajima, Y. Honda, O. Kitao, H. Nakai, T. Vreven, K. Throssell, J. A. Montgomery Jr., J. E. Peralta, F. Ogliaro, M. J. Bearpark, J. J. Heyd, E. N. Brothers, K. N. Kudin, V. N. Staroverov, T. A. Keith, R. Kobayashi, J. Normand, K. Raghavachari, A. P. Rendell, J. C. Burant, S. S. Iyengar, J. Tomasi, M. Cossi, J. M. Millam, M. Klene, C. Adamo, R. Cammi, J. W. Ochterski, R. L. Martin, K. Morokuma, O. Farkas, J. B. Foresman and D. J. Fox, Gaussian 16 Rev. C.01.*Journal*, 2016.

(17) Y. Zhao and D. G. Truhlar, The M06 suite of density functionals for main group thermochemistry, thermochemical kinetics, noncovalent interactions, excited states, and transition elements: two new functionals and systematic testing of four M06-class functionals and 12 other functionals, *Theoretical chemistry accounts*, 2008, **120**, 215-241.

(18) W. J. Hehre, R. Ditchfield and J. A. Pople, Self—consistent molecular orbital methods. XII. Further extensions of Gaussian—type basis sets for use in molecular orbital studies of organic molecules, *The Journal of Chemical Physics*, 1972, **56**, 2257-2261.

(19) J. Tomasi and M. Persico, Molecular interactions in solution: an overview of methods based on continuous distributions of the solvent, *Chemical Reviews*, 1994, **94**, 2027-2094.

(20) T. Lu and F. Chen, Multiwfn: A multifunctional wavefunction analyzer, *Journal of computational chemistry*, 2012, **33**, 580-592.

(21) Z. Liu, T. Lu and Q. Chen, An sp-hybridized all-carboatomic ring, cyclo [18] carbon: Electronic structure, electronic spectrum, and optical nonlinearity, *Carbon*, 2020, **165**, 461-467.

(22) J. Zhang and T. Lu, Efficient evaluation of electrostatic potential with computerized optimized code, *Physical Chemistry Chemical Physics*, 2021, **23**, 20323-20328.

(23) C. I. Bayly, P. Cieplak, W. Cornell and P. A. Kollman, A well-behaved electrostatic potential based method using charge restraints for deriving atomic charges: the RESP model, *The Journal of Physical Chemistry*, 1993, **97**, 10269-10280.